Aerosol pH Indicator and Organosulfate Detectability from Aerosol Mass Spectrometry

Measurements

Melinda K. Schueneman[1], Benjamin A. Nault[1,a], Pedro Campuzano-Jost[1], Duseong S. Jo[1,2], Douglas A. Day[1], Jason C. Schroder[1,b], Brett B. Palm[1], Alma Hodzic[2], Jack E. Dibb[3], and Jose L. Jimenez[1]

[1] Department of Chemistry, and Cooperative Institute for Research in Environmental Sciences (CIRES), University of Colorado, Boulder, CO, USA
[2] Atmospheric Chemistry Observations and Modeling, National Center for Atmospheric Research, Boulder, CO 80301, USA
[3] Earth Systems Research Center, Institute for the Study of Earth, Oceans, and Space, University of New Hampshire, USA

a. Now at: Aerodyne Research, Inc., Billerica, MA, USA
b. Now at: Air Pollution Control Division, Colorado Department of Public Health and the Environment, Denver, CO, USA

Correspondence: jose.jimenez@colorado.edu

Abstract

Aerosol sulfate is a major component of submicron particulate matter (PM_1). Sulfate can be present as inorganic (mainly ammonium sulfate, AS) or organosulfate (OS). Although OS is thought to be a smaller fraction of total sulfate in most cases, recent literature argues that this may not be the case in more polluted environments. Aerodyne Aerosol Mass Spectrometers (AMS) measure total submicron sulfate, but it has been difficult to apportion AS vs. OS as the detected ion fragments are similar. Recently, two new methods have been proposed to quantify OS separately from AS with AMS data. We use observations collected during several airborne field campaigns covering a wide range of sources and airmass ages (spanning the continental US, marine remote troposphere, and Korea) and targeted laboratory experiments to investigate the performance and validity of the proposed OS methods. Four chemical regimes are defined to categorize the factors impacting sulfate fragmentation. In polluted areas with high ammonium nitrate concentrations and in remote areas with high aerosol acidity, the decomposition and fragmentation of sulfate in the AMS is influenced by multiple complex effects, and estimation of OS does not seem possible with current methods. In regions with lower acidity (pH>0) and ammonium nitrate (fraction of total mass<0.3), the proposed OS methods might be more reliable,

although application of these methods often produced nonsensical results. However, the fragmentation of ambient neutralized sulfate varies somewhat within studies, adding uncertainty, possibly due to variations in the effect of organics. Under highly acidic conditions (when calculated pH<0 and ammonium balance<0.65), sulfate fragment ratios show a clear relationship with acidity. The measured ammonium balance (and to a lesser extent, the $H_ySO_x^+/SO_x^+$ AMS ratio) is a promising indicator for rapid estimation of aerosol pH < 0, including when gas-phase NH_3 and HNO_3 are not available. These results allow an improved understanding of important intensive properties of ambient aerosols.
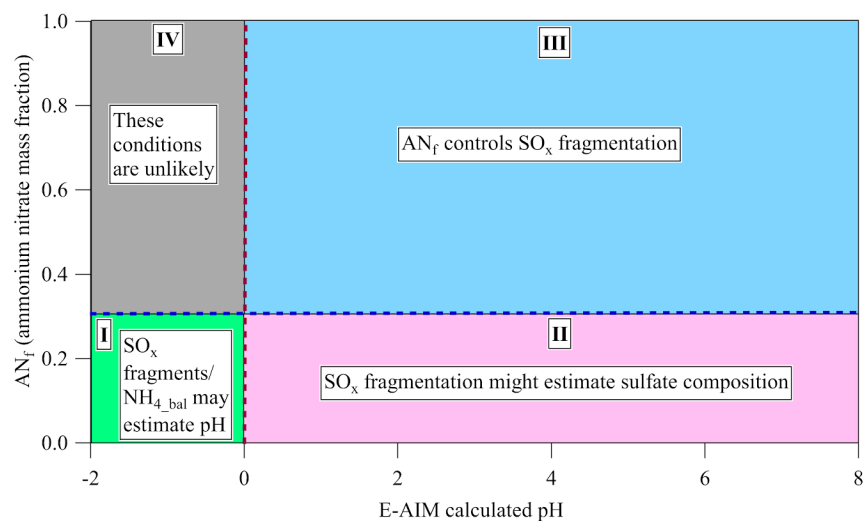
Introduction

PM$_1$, or submicron aerosols, have important impacts on visibility, climate, and environmental and human health (Dockery et al., 1996; Lighty et al., 2000; Lohmann et al., 2004; IPCC, 2013). In order to quantify the impacts of PM$_1$, and their evolution with changes in emissions, chemistry, and climate, PM$_1$ sources, chemistry, and composition must be understood. Field measurements are critical to that goal, and one tool used extensively in field studies since the early 2000s is the Aerodyne Aerosol Mass Spectrometer (AMS) and more recently its simplified version, the Aerosol Chemical Speciation Monitor (ACSM) (Jayne et al., 2000; DeCarlo et al., 2006; Canagaratna et al., 2007; Ng et al., 2011a). The AMS typically quantifies the chemical composition and size distribution of sulfate, nitrate, organic aerosol (OA), ammonium, and chloride (Jayne et al., 2000; DeCarlo et al., 2006; Canagaratna et al., 2007; Jimenez et al., 2009).

Within the AMS, particles are vaporized, leading to some thermal decomposition (e.g., (Docherty et al., 2015) and then ionized via 70 eV electron ionization, which leads to substantial fragmentation of the molecular ions. Despite or perhaps because of the substantial (and reproducible) decomposition and fragmentation, the relative signals of different AMS fragments have been found to be indicative of different chemical species in the aerosol. These include the presence of inorganic vs. organic nitrates (Farmer et al., 2010; Fry et al., 2013), and of several source and composition characteristics of organic aerosols (Alfarra et al., 2004; Zhang et al., 2004a; Cubison et al., 2011; Ng et al., 2011b; Hu et al., 2015). In contrast to nitrates, deconvolving inorganic vs. organosulfates (OS, which includes sulfonic acids, when present) is thought to be more difficult. The fragmentation pattern for one atmospherically relevant OS was

similar to those of inorganic sulfates (mainly ammonium-sulfate salts, AS) in an early study, with minimal C-S-containing fragments (Farmer et al., 2010). Until recently, most studies have shown that the OS molar fraction (OS_f = OS / (AS + OS), calculated using only the sulfate moiety of the molecules) typically makes a small (~1-10%) contribution to total sulfate in PM_1 (e.g. Tolocka and Turpin, 2012; Hu et al., 2015; Liao et al., 2015; Riva et al., 2016, 2019). However, for biogenic areas OS_f is predicted to increase substantially in the future (Riva et al., 2019). Another important recent subject of debate is the missing sources of sulfate production in haze events in China (Wang et al., 2014; Zheng et al., 2014; Li et al., 2017), which some studies have attributed to a major contribution of OS (e.g., Song et al., 2019). It should be noted that a recent study reports that OS filter-based measurements in past scientific studies may have substantial associated positive biases, leading to an overestimate for [OS] (Brüggemann et al., 2020). It is also important to quantify OS in order to understand the chemistry of aerosol formation and aging (Surratt et al., 2007, 2008; Song et al., 2019), which impacts the ability to understand how sulfate may influence various PM_1 properties and processes (e.g., gas uptake, aqueous reactions). Finally, accurate AS concentrations are needed to quantify the inorganic:organic ratio (to predict the hygroscopicity of PM_1, which impacts satellite and model interpretation) and to estimate aerosol pH and liquid water content from thermodynamic models, as it is currently still not possible to measure the aerosol pH in the field in-situ (Hennigan et al., 2015; Guo et al., 2016; Craig et al., 2018; Pye et al., 2019).

Recent AMS work has attempted to quantify OS_f from the measured individual sulfate ion signals (Chen et al., 2019; Song et al., 2019). The vaporization and ionization of AS and OS in the AMS produce similar ion fragments that do not contain a carbon atom, the major ones

95 quantified being SO^+, SO_2^+, SO_3^+, HSO_3^+, and $H_2SO_4^+$. These ions were attributed primarily to

96 inorganic sulfate in earlier AMS analyses (e.g. Jimenez et al. 2003), but were shown to have a

97 contribution from organosulfates by (Farmer et al., 2010). Note that these are the ions detected in

98 the AMS (following ionization/decomposition), and not the ions present in the aerosols

99 (discussed in Sect. 3.3 and shown in Fig. 2C). However, a recent laboratory study with many OS

100 standards found reproducible differences in the fragmentation of AS vs OS (Chen et al., 2019).

101 That study proposed a method using the unique AS ion fragments ($H_2SO_4^+$ and HSO_3^+) divided

102 by the total sulfate signal ($H_2SO_4^+ +HSO_3^++SO_3^++SO_2^++SO^+$) to apportion OS, AS, and

103 methylsulfonic acid (MSA, an organosulfur compound, but not an organosulfate) in field

104 datasets. It is important to note that MSA can be directly measured with the (HR-)AMS (Phinney

105 et al., 2006; Zorn et al., 2008; Huang et al., 2017; Hodshire et al., 2019), so quantification of

106 MSA with the method in Chen et al. is not necessary. From this method, an average OS mass

107 concentration (C_{OS}) of 0.12 µg m^{-3} was estimated for the Southern Oxidant and Aerosol Study

108 (SOAS) ground campaign in rural Alabama (Carlton et al., 2018), with $OS_f \sim 4\%$ (Chen et al.,

109 2019). That estimate is consistent with others for that site and region (Hu et al., 2015; Liao et al.,

110 2015). An alternative method to estimate OS_f based on the same principle was proposed by Song

111 et al. (2019) using the observed AMS $SO^+/H_ySO_x^+$ and $SO_2^+/H_ySO_x^+$. These authors reported

112 $OS_f \sim 17\% \pm 7\%$ (which corresponds to [OS] $\sim$ 5-10 µg m^{-3}) during winter haze episodes in China.

113 A recent study (Dovrou et al., 2019) investigated mixtures of sodium sulfate and sodium

114 hydroxymethanesulfonate (HMS); however, they found that HMS cannot be distinguished from

115 AMS ions alone, due to the complex ambient aerosol mixture containing organosulfates, and

116 inorganic sulfates, which all, in part, produce the same sulfate fragments as HMS.

117   Another important and related analytical challenge is online quantification or estimation

118 of ambient aerosol acidity from real-time measurements, e.g. during field campaigns. So far,

119 online aerosol pH measurements have only been performed in the laboratory (Rindelaub et al.,

120 2016; Craig et al., 2018). Aerosol acidity is important because it impacts human health by

121 decreasing lung function (Raizenne et al., 1996), and strongly impacts the equilibria and kinetics

122 of a very large number of atmospheric physical and chemical processes (Jang et al., 2002;

123 Meskhidze et al., 2003; Anon, 2007; Thornton et al., 2008; Bertram and Thornton, 2009; Gaston

124 et al., 2014; Ackendorf et al., 2017; Guo et al., 2017; Losey et al., 2018). In addition, the

125 deposition of acidic particles leads to damage to terrestrial and freshwater ecosystems, i.e. "acid

126 rain" or more properly acid deposition (Schindler, 1988; Johnson et al., 2008). Currently, the

127 state-of-the art technique to quantify aerosol acidity for field data is to run an inorganic aerosol

128 thermodynamic model that includes the measured particle and gas inorganic concentrations, as

129 well as temperature and humidity. The Extended Aerosol Inorganics Model (E-AIM) (Clegg et

130 al., 1998a, 2003; Wexler and Clegg, 2002) is generally considered as the reference model (Pye et

131 al., 2019). ISORROPIA-II (Nenes et al., 1999; Fountoukis and Nenes, 2007) is a faster model

132 utilizing look-up tables to calculate aerosol liquid water content (and thus is frequently used as

133 part of chemical transport models) at the expense of some accuracy at different RH levels (Pye et

134 al., 2019). In general, these thermodynamic models are thought to perform best for pH estimation

135 when gas-phase measurements of NH_3 and/or HNO_3 are used in the calculations, and to perform

136 less well when run only with aerosol measurements (Guo et al., 2015; Hennigan et al., 2015;

137 Song et al., 2018).

There has been an ongoing debate about the potential relationship between the inorganic cation/anion charge ratio (commonly referred to as "ammonium balance", see Eq. (4)) and aerosol acidity. Ammonia gas and its particle phase equivalent (ammonium) are the dominant bases in the atmosphere (Dentener and Crutzen, 1994). As the most important base in PM_1, a deficit of NH_4^+ vs. dominant PM_1 anions, SO_4^{2-} and NO_3^- (Jimenez et al., 2009), is indicative of the concentration of H^+, since the particles are (nearly) electrically neutral. Thus, in the absence of substantial non-volatile cations (e.g. Na^+, K^+) ammonium balance is an indicator of aerosol acidity. Ammonium balance has been shown to correlate well with pH under certain conditions, specifically, when using daily averaged temperature and relative humidity (Zhang et al., 2007a), but has been criticized as being a poor surrogate of pH under other conditions (Hennigan et al., 2015). In particular, ammonium balance can be a poor surrogate of pH because changes in T and RH impact the aerosol liquid water in the diurnal cycle (Zhang et al., 2007a). This is especially important in the boundary layer where almost all past pH quantification has been carried out (Pye et al., 2019), compared to the lower diurnal variance of T and RH in the free and upper troposphere. Many field studies do not include measurements of NH_3 or HNO_3, two species that are difficult to measure due to inlet delays caused by strong interactions with surfaces. Both species are typically present at low concentrations and thus not routinely measured, limiting the ability to calculate aerosol pH (Hennigan et al., 2015). A more direct estimate of aerosol acidity using only ambient particle data is highly desirable.

Here, we analyze sulfate ion fragment data from laboratory and ambient AMS observations, spanning multiple aircraft campaigns with a routinely calibrated AMS response to AS, and across a wide range of chemical and meteorological environments. We use this large

160 dataset to test the applicability of recently published methods to partition AS and OS. We

161 investigate the feasibility of estimating pH based on AMS data; as well as the regions of

162 chemical space where the different estimation methods may work. Finally, we provide a physical

163 interpretation for sulfate fragmentation in the AMS.

164 **2 Methods**

165 **2.1 Airborne Campaigns**

166   Sulfate fragmentation data was obtained using an Aerodyne High-Resolution

167 Time-of-Flight Aerosol Mass Spectrometer (AMS) (Aerodyne Research Inc., Billerica, MA,

168 USA; (DeCarlo et al., 2006)). The ambient data used here are from aircraft observations from the

169 following campaigns (Table 1): DC3 (Barth et al., 2015), SEAC[4]RS (Toon et al., 2016),

170 WINTER (Schroder et al., 2018), KORUS-AQ (Nault et al., 2018), and ATom-1 and ATom-2

171 (Guo et al., 2020; Hodzic et al., 2020). Flight paths for all six campaigns are shown in Fig. S1.

172 These campaigns span polluted urban, partially polluted biogenic, biomass burning smoke, rural,

173 and remote regions of the atmosphere. DC3 sampled continental / rural conditions with diffuse

174 pollution and some biomass burning events. WINTER and KORUS-AQ were airborne

175 campaigns that focused on urbanized regions (although from different regions and times of year

176 (Table 1)); therefore, the campaigns had appreciable mass concentrations of ammonium nitrate

177 due to anthropogenic emissions of NO_x and the subsequent production of HNO_3 that partitions

178 into the aerosol with ammonia (Seinfeld and Pandis, 2006). SEAC[4]RS focused on regional

179 background chemistry of the continental United States, which included impacts from biomass

180 burning, biogenic, and pollution emissions, and upper tropospheric chemistry impacted by

181 convection. Finally, ATom-1 and ATom-2 sampled the remote Pacific and Atlantic basins with

182 continuous full vertical profiling, in order to study the composition of the remote marine

183 atmosphere, impacted by long range transported chemical species and marine emissions, and far

184 from anthropogenic sources. Not all campaigns are usable for all the analyses in this paper,

185 depending on the quality and completeness of the data. Table 1 indicates which campaigns were

186 usable for each analysis.

187 **2.2 High-Resolution Time-of-Flight Aerosol Mass Spectrometer**

188   The highly customized University of Colorado-Boulder aircraft AMS was used in all

189 campaigns and has been described elsewhere (DeCarlo et al., 2008; Dunlea et al., 2009; Nault et

190 al., 2018; Schroder et al., 2018; Guo et al., 2020), so only details relevant to this study are

191 summarized here. Ambient air is drawn through a National Center for Atmospheric Research

192 (NCAR) High-Performance Instrumented Airborne Platform for Environmental Research

193 Modular Inlet (HIMIL: (Stith et al., 2009)) with a constant standard flow rate of 9 L min^{-1}, and

194 all data is reported at a constant standard temperature (T = 273 K) and pressure (P = 1013 hPa).

195 The sampled air enters a pressure controlled inlet (Bahreini et al., 2008) and is then introduced

196 into an aerodynamic focusing lens (Liu et al., 1995; Zhang et al., 2004b). Particles then impact

197 onto an inverted cone porous tungsten "standard" vaporizer, operated at ~ 600 °C under high

198 vacuum. The standard vaporizer is used in this study. A "capture vaporizer" has been recently

199 demonstrated, it leads to more thermal decomposition while still retaining similar (although

200 noisier) fragment information (Hu et al., 2017a; Zheng et al., 2020), but it is not used here.

201 Non-refractory species, those that evaporate in less than a few seconds (such as sulfate, nitrate,

ammonium, and organic material), are subsequently ionized by 70 eV electrons. Some refractory

and semi-refractory species such as sea-salt, lead and potassium can be detected by the AMS in

some cases (Lee et al., 2010; Salcedo et al., 2010; Ovadnevaite et al., 2012; Hodzic et al., 2020)).

A cryopump reduces background in the ionizer by orders of magnitude during the flights, leading

to low detection limits, in particular for NH_4, which is critical for acidity quantification in the

remote troposphere. Data was taken at 1 Hz, but was processed at both 1 Hz and 1 minute

resolution, and the latter product is primarily used here due to higher signal-to-noise ratios. The

one minute datasets were further filtered by removing points where the sulfate signal was below

three times its detection limit. Detection limits were estimated continuously via the methods of

Drewnick et al. (2009), and confirmed with frequent in-flight filter blanks. For the laboratory

studies, everything was kept the same as on the aircraft other than no use of the HIMIL aircraft

inlet. Data was processed and analyzed with the standard Squirrel and PIKA ToF-AMS data

analysis software packages within Igor Pro 7 (Wavemetrics) (DeCarlo et al., 2006; Sueper,

2018).

One important parameter for AMS quantification is collection efficiency (CE). CE is the

probability that a particle entering the AMS is detected. It is affected by several particle

properties (Huffman et al., 2005), the most important being particle bounce off the vaporizer

without detection (Middlebrook et al., 2012). Bounce is controlled by particle phase (Quinn et

al., 2006; Matthew et al., 2008), and is estimated for ambient particles based on their ammonium

balance (acidity) and ammonium nitrate content (Middlebrook et al., 2012). This

parameterization performs well for ambient particles (Middlebrook et al., 2012; Hu et al., 2017a,

2020; Guo et al., 2020). Still, potential variability in CE that is not perfectly captured by the

224 parameterization contributes a major fraction of the AMS uncertainty for ambient particle

225 analysis (Bahreini et al., 2009). Alternative methods to estimate ambient CE for ambient

226 particles are of interest, we explore a potential alternative method here.

227 **2.3 Quantification of OS/AS using Literature Methods**

228   Two methods have been proposed to quantify OS contribution to total sulfate using AMS

229 sulfate ion fragment fractions. The first method uses different sulfate ions to attribute measured

230 total sulfate to either OS, AS, or methanesulfonic acid (MSA). Due to the structure of OS, only

231 non-hydrogenated sulfate ions, i.e., SO^+, SO_2^+ and SO_3^+, are produced in the AMS for OS. AS

232 does produce hydrogenated sulfate ions, i.e., $H_2SO_4^+$ and HSO_3^+, as well as the same

233 non-hydrogenated sulfate ions produced by OS. Chen et al. (2019) proposed a "triangle method"

234 to estimate these two species and MSA, based on the observed fragments. Note that mineral

235 sulfates such as sodium sulfate fragment similarly to OS, and thus these methods need to be

236 interpreted differently in regions with significant submicron mineral sulfates. MSA calibrations

237 show variability for the fragments (Chen et al., 2019), and were not performed for all the studies

238 in this work. Since MSA can be quantified without using the sulfate fragments, here we apply

239 this method to estimate the fractions of OS and AS by using a one dimensional version of the

240 triangle (i.e. just the hypotenuse connecting pure OS to pure AS). An alternative method is

241 based on the same assumptions, but uses different equations to quantify the relative

242 concentration of OS (Song et al., 2019).

243   Both literature methods for deconvolving sulfate as OS and AS assume that the main

244 factor impacting sulfate fragmentation in the AMS is sulfate structure (OS, AS, or MSA). Chen

245 et al. (2019) briefly mention that acidity can impact sulfate fragmentation, but this effect has not

246 been studied and quantified. In addition, Chen et al. (2019) used pure standards to quantify the

247 AMS fragmentation of different species, but did not explore potential matrix effects in AMS

248 fragments which could impact internally mixed ambient particles.

249 **2.4 Quantification of the AMS Sulfate Fragment Ratios**

250   To compare our field data to that analyzed in Chen et al. (2019) we use the variables

251 defined in that study, $fH_2SO_4^+$ and $fHSO_3^+$ and define the normalized $nfH_2SO_4^+$ and $nfHSO_3^+$

252 (normalized to the values of $fH_2SO_4^+$ and $fHSO_3^+$ for pure AS) :

$$fH_2SO_4^+ = \frac{[H_2SO_4^+]}{[H_2SO_4^+]+[HSO_3^+]+[SO_3^+]+[SO_2^+]+[SO^+]} \qquad \text{Eq. 1}$$

$$nfH_2SO_4^+ = \frac{fH_2SO_4^+}{fH_2SO_4^+ \text{ (pure AS)}} \qquad \text{Eq. 2}$$

$$fHSO_3^+ = \frac{[HSO_3^+]}{[H_2SO_4^+]+[HSO_3^+]+[SO_3^+]+[SO_2^+]+[SO^+]} \qquad \text{Eq. 3}$$

$$nfHSO_3^+ = \frac{fHSO_3^+}{fHSO_3^+ \text{ (pure AS)}} \qquad \text{Eq. 4}$$

253 It should be noted that while that study includes methanesulfonic acid (MSA) data, the impact of

254 MSA on $fH_2SO_4^+$ and $fHSO_3^+$ is minimal for the ATom campaigns (see Fig. S2). Additionally,

255 one study over the Western United States (representing a rural, continental region) observed

256 MSA concentrations of ~50 ng m^{-3} (Sorooshian et al., 2015), which results in a very small

257 deviation in the Chen triangle and can hence be neglected for the purposes of this work. All

258 variables were normalized to the values of the same variables for pure AS calibrations

259 (conducted during each field experiment) in order to eliminate some of the spread in the sulfate

260 ions that is likely due to instrument-to-instrument or instrument-in-time variability (Fry et al.,

261 2013; Chen et al., 2019) (Fig. S3) . We also define a new AMS sulfate ion ratio, $H_ySO_x^+/SO_x^+$,

262 and create the normalized $nH_ySO_x^+/SO_x^+$ to reduce the influence of instrument-to-instrument or

263 instrument-in-time variability:

$$H_ySO_x^+/SO_x^+ = \frac{[HySO_x^+]}{[SO_x^+]} = \frac{[H_2SO_4^+]+[HSO_3^+]}{[SO_3^+]+[SO_2^+]+[SO^+]} \qquad \text{Eq. 5}$$

$$nH_ySO_x^+/SO_x^+ = \frac{H_ySO_x^+/SO_x^+}{H_ySO_x^+/SO_x^+ \ (pure \ AS)} \qquad \text{Eq. 6}$$

264 The submicron aerosol molar Ammonium Balance (NH_{4_bal}) is calculated as:

$$NH_{4\_bal} = \frac{[NH_4]/18}{([SO_4]/48)+([NO_3]/62)+([Chl]/35)} \qquad \text{Eq. 7}$$

265 The concentration of non-refractory chloride is only included for non-remote campaigns

266 (KORUS-AQ, WINTER, and SEAC⁴RS), since it was negligible for others and strongly

267 impacted by seasalt in the marine boundary layer. The fraction of ammonium nitrate in the

268 particle phase (ammonium nitrate mass fraction, AN_f) (by mass):

$$AN_f = \frac{(80 \div 62) \times [Inorganic \ NO_3]}{[NO_3]+[SO_4]+[NH_4]+[Chl]+[Org]} \qquad \text{Eq. 8}$$

269 The fraction of total AMS aerosol mass comprised of OA (OA_f) is:

$$OA_f = \frac{[Org]}{[NO_3]+[SO_4]+[NH_4]+[Chl]+[Org]} \qquad \text{Eq. 9}$$

270 The sulfate equivalent concentration of OS in the Song et al. (2019) paper is calculated as:

$$C_{OS} = M_{SO_4^{2-}}\left[\frac{SO_{obs}^+ - R_{cd,\,SO^+/H_ySO_x^{+,*}} \cdot H_ySO_{x,\,obs}^{+,*}}{M_{SO^+}} + \frac{SO_{2,\,obs}^+ - R_{cd,\,SO_2^+/H_ySO_x^{+,*}} \cdot H_ySO_{x,\,obs}^{+,*}}{M_{SO_2^+}}\right] \qquad \text{Eq. 10}$$

271 where "cd" stands for "clean and dry". Clean and dry conditions are defined in Song et al. (2019)

272 as ambient data points where $PM_1 = 10\ \mu g\ m^{-3}$ and RH = 30%. Clean and dry conditions are

273 assumed to represent nearly pure AS. M is for the molar mass of the different sulfate ions, and

274 "obs" represents the ambient data for specific sulfate fragments. $H_ySO_x^{+,*}$ (which differs from the

275 notation used in Song's paper, but is necessary to differentiate $H_ySO_x^+$ between the Chen and

276 Song papers) is defined in Song et al. (2019) as $(SO_3^+ + HSO_3^+ + H_2SO_4^+)$. For the Chen method,

277 the C_{OS} is defined based on the AS normalized $nfH_2SO_4^+$ values:

$$C_{OS} = [SO_4] - nfH_2SO_4^+ * [SO_4] \qquad \text{Eq. 11}$$

278 OS_f, the fraction of OS:total sulfate is defined as:

$$OS_f = \frac{C_{OS}}{[SO_4]} \qquad \text{Eq. 12}$$

279 Where C_{OS} is calculated from Eq. (10) or Eq. (11).

2.5 Laboratory Experiments

281   As ambient aerosols contain mixtures of chemical species, we investigated if matrix

282 effects may impact the fragmentation of sulfate species. Different solution mixtures, composed

283 of various amounts of AS (Certified ACS, 99.7% purity) and ammonium nitrate (AN) (Certified

284 ACS, 99.9% purity) in water (Milli-Q grade (R > 19 MOhms)) were atomized to generate

285 particles and size selected using a Differential Mobility Analyzer (DMA) (TSI Model 3081),

286 analyzed with a Condensation Particle Counter (CPC) (Model 3775), and electrostatic classifier

287 (Model 3080), for mobility diameters between 350-400 nm. We investigated AS/AN mixtures,

288 ranging from $AN_f = 0\%$ to 95%.

289   In order to assess effects on the sulfate fragmentation from mixing with OA, chamber

290 experiments, where different types of SOA were formed by gas-phase reactions and

291 condensation onto AS seeds, were investigated. SOA was formed from alkanol and toluene

292 photooxidation under high-NO_x conditions (Liu et al., 2019), as well as Δ-3-carene and α-pinene

293 reactions with nitrate radicals Kang et al. (2016). Experiments were initiated with 100% AS in a

294 dry chamber (RH < 5%; ~ 298 K) followed by either rapid, gradual, or stepwise increases of

295 SOA until a maximum OA/(OA+AS) ratio of ~ 70% was reached. Aerosol composition was

296 monitored by AMS and size distributions were monitored with a scanning mobility particle sizer

297 (SMPS: DMA was TSI Model 3081, electrostatic classifier was Model 3080, and the CPC was

298 Model 3775). RIE of sulfate was directly calibrated with pure ammonium sulfate, while RIE *

299 CE of the SOA produced was estimated by comparison to the SMPS integrated volume, together

300 with OA density estimated from the AMS-derived elemental ratios per Kuwata et al. (2012)), in

301 order to accurately quantify OA/(OA+AS). Humid experiments were not considered here due to

302 the potential of forming organosulfates.

303 **2.6 E-AIM Thermodynamic Model for pH Estimation**

304   Aerosol pH was estimated using the Extended Aerosol Inorganic Model (E-AIM) Model

305 IV (Clegg et al., 1998b; Massucci et al., 1999; Wexler and Clegg, 2002). We input into the model

306 (ran in "forward mode"), the total nitrate (gas-phase HNO_3 plus particle-phase total NO_3^-),

307 sulfate, ammonium, relative humidity (calculated according to the parameterization of Murphy

308 and Koop (2005), which is critical for upper tropospheric conditions), and temperature. Total

309 nitrate (inorganic+organic) was input, as Nault et al. (2021) found that removing estimated

310 organic nitrate does not impact the pH calculation. This was done to calculate aerosol liquid

311 water and aerosol pH. Model IV was not run with chloride ions, as their concentrations were

312 very low, and including chloride limits the model to temperatures ≥ 263 K (Friese and Ebel,

313 2010), which would greatly limit the analysis of calculated pH for WINTER, ATom-1, and

314 ATom-2. We have added the modifier "calculated" before pH for all situations where we are

315 describing the E-AIM pH, and "estimated" when we refer to pH from the empirical estimation

316 methods from AMS measurements, introduced in this study. Also, including chloride precludes

317 running the model under supersaturated solution conditions, which is a closer approximation of

318 ambient aerosol (Pye et al., 2019). All aerosol mass concentrations were from the CU AMS.

319 $HNO_3(g)$ was measured by the California Institute of Technology chemical ionization mass

320 spectrometer (CIT-CIMS) (Crounse et al., 2006), which was flown in all of these missions

321 (excluding WINTER, where the UW-CIMS was used for the HNO_3 measurements) (Lee et al.,

322 2014, 2018). Results are generally similar when using the SAGA mist chamber measurement for

323 total nitrate (Nault et al., 2020). The forward mode is less sensitive to uncertainties in

324 measurements than the "reverse mode," which only uses particle composition and T/RH as

325 inputs (Hennigan et al., 2015). Also, due to lack of $NH_3(g)$ measurements, the model was run

326 iteratively until convergence in modeled NH_3 occurred, similar to Guo et al. (2016). Performance

327 for calculated pH was investigated by comparing model-calculated HNO_3 and NO_3^- to

328 measurements, as the partitioning of nitrate between gas- and particle-phase is sensitive to

329 calculated pH under acidic conditions (Guo et al., 2016). For all campaigns included herein

330 (DC3, WINTER, SEAC^{4}RS, KORUS-AQ, ATom-1, and ATom-2), the slopes of HNO_3

331 (measured vs. predicted) are within the uncertainty of the measurements; with good correlations

332 (SI Fig. S4). For NO_3^-, the slopes are within the measurement uncertainty for five of the six

333 campaigns. For ATom-2, the NO_3^- slopes were low; however, for this campaign, the measured

334 NO_3^- mass concentrations were extremely low (mean = 0.02 µg sm^{-3}), and the calculated pH was

335 also very low (mean = - 0.5), leading to very little NO_3^- in the aerosol phase (see SI Fig. S4).

336   In addition, other bases present in the atmosphere (such as amines) were examined. Prior

337 studies have shown that amines were less than a maximum concentration of 30 ng m^{-3} at the

338 ocean surface (Gibb et al., 1999; Facchini et al., 2008; Müller et al., 2009; Frossard et al., 2014;

339 van Pinxteren et al., 2015; Youn et al., 2015). Another study by Sorooshian et al., (2009) found

340 that amine mass concentration dropped off quickly with altitude to concentrations less than 25 ng

341 m^{-3} at an altitude between 200 and 300 m, which is the approximate minimum altitude flown on

342 the DC-8 during the ATom campaigns. As the one minute detection limit for the AMS data for

343 amines is typically 10 ng m^{-3}, we expect the amine signal to generally be below the limit of

344 detection, and thus outside of our quantification capabilities. This was observed for AMS data

345 from the ATom campaigns, using characteristic ions identified in past studies (Murphy et al.,

346 2007; Ge et al., 2014). It was found that amine ions cannot be distinguished from background for

347 many ATom flights. Only during one flight in ATom-1, we observed an amine signal ($C_2H_6N^+$

348 m/z = 44) above the background (see SI Fig. S5). During this flight, amines (from the

349 contribution of CH_4N, C_2H_6N, and C_3H_8N) only accounted for 0.7 ng m^{-3} of aerosol, whereas

350 ammonium accounted for 19 ng m^{-3}. Amines can produce the same fragments as ammonium, but

351 this is only the case for a few percent of the amine fragments (Ge et al., 2014). In this case, the

352 ammonium concentration is 25 times that of the amines. Since amines were even lower during

353 other flights, we assume the effect of amines to the pH calculation is very small and can be

354 ignored for E-AIM calculations.

355 **2.7 GEOS-Chem Model**

356   We used a global chemical transport model (GEOS-Chem 12.6.1,

357 doi:10.5281/zenodo.3520966; (Bey et al., 2001)) to investigate modeled global distributions of

358 ammonium nitrate mass fraction (AN_f) and calculated aerosol pH across different regions.

359 GEOS-Chem was driven by assimilated meteorological fields from the Modern-Era

360 Retrospective analysis for Research and Applications version 2 (MERRA2) (Gelaro et al., 2017)

361 for the year of 2010. The simulation was conducted at 2° (latitude) × 2.5 (longitude) with 47

362 vertical layers up to 0.01 hPa and ~30 layers under 200 hPa. We used the Community Emissions

363 Data System (CEDS) inventory for global anthropogenic emissions (Hoesly et al., 2018) and the

364 global fire emissions database version 4 (GFED4) for biomass burning emissions (Giglio et al.,

365 2013). Aerosol pH and gas-particle partitioning of inorganic aerosols were calculated online

366 using the ISORROPIA-II model within GEOS-Chem (Fountoukis and Nenes, 2007; Pye et al.,

367 2009). Similar to Jo et al., (2019) sea salt aerosol was excluded from pH calculations based on a

368 better agreement with the observationally-constrained calculated pH values as suggested by

369 Nault et al. (2020). Oceanic NH_x emissions were also included in this model based on recent

370 work (Paulot et al., 2015; Nault et al., 2020).

371 **3 Results and Discussion**

3.1 Lab quantification of AMS data

Application of the one dimensional Chen method to laboratory data is shown in Fig. 1.

Data are expected to lie inside the triangular region, and be apportioned depending on the

relative distance to the three vertices. For example, data lying at [0.5,0.5] on the line between the

OS and AS points would represent a sample with ~50% OS and ~50% AS. If data clusters

around the [1,1] point where pure AS resides, all of the sulfate is attributed to AS. From applying

this method, it is clear that none of the campaign averages or laboratory data falls between the

[0,0] and [1,1] points, suggesting that there may be additional factors (other than sulfate

composition) impacting the location of data in this triangular region.

The effect of internally mixed ammonium nitrate (AN) is shown in Fig. 1A. For mixtures

containing $AN_f < 50\%$, data centers around the pure AS point in the Chen triangle. When AN_f is

increased past 0.50, there is an increase in both $nfH_ySO_x^+$ ions, even when all of the particulate

sulfate is inorganic. As the particle AN_f increases up to AN_f=0.95, the OS_f estimation becomes

increasingly inaccurate. The method may estimate OS_f=0% in the latter situation, when OS_f is

actually 50%. While OS_f=0% may be reasonable in some parts of the atmosphere, and one may

be inclined to accept this result as it is non-negative, it is actually incorrect due to the effect of

particulate AN. Thus for laboratory data, the Chen method should not be used on mixtures

containing $AN_f > 0.50$.

The effect of OA internally mixed with AS on the sulfate fragmentation pattern was also

explored with toluene, alkanol, and monoterpene SOA (Fig. 1B and Fig. S6). For the alkanol

SOA experiments we found that the presence of even a small coating of alkanol SOA (which is

thought to be liquid (Liu et al., 2019)) shifts the normalized AS [1,1] point to ~[1.08,1.08], but

394 increases in the fraction of OA (OA_f) from 0.1 to 0.3 lead to no further changes in $nfH_ySO_x^+$ (Fig.

395 1B). This means that for a sample containing a mixture of AS and alkanol SOA, the calculated

396 OS_f would be -15% (Chen). In contrast, toluene SOA, which spans $0 < OA_f < 0.5$, shows no

397 clear change in the $nfH_ySO_x^+$ ions, indicating that OA_f would not bias the Chen method for this

398 example. The monoterpene SOA, from two different experimental datasets (2014 and 2015)

399 using different AMSs, show more varied results than the previous two studies. Overall, the 2014

400 data shows a very small increase in the "pure" AS value in the OA_f range 0-0.50, whereas the

401 2015 monoterpene data shows a consistent and constant 10-20% increase in $nfH_ySO_x^+$ compared

402 to the pure AS calibration point (similarly to the alkanol SOA). However, when OA_f is in the

403 range of $0.50<OA_f<0.70$, 30-40% increases are observed for the 2014 and 2015 data. This result

404 is only applicable to a few of the experiments (see Fig. S6), potentially due to very high SOA

405 loadings (up to 300 μg m^{-3}). These high OA concentrations could potentially lead to a change of

406 the particle phase due to condensation of more volatile and liquid species, potentially altering the

407 interactions of the particles and the vaporizer surfaces. These experiments collectively suggest

408 that a "pure" AS calibration point of [1.15,1.15] may be more appropriate when applying the

409 Chen et al. method to some mixed aerosol at typical OA concentrations observed in the

410 atmosphere; this is discussed further in Sect. 3.2.

411   Chen et al. briefly discussed the potential impact of acidity on their OS quantification

412 method. This is explored here with pure sulfuric acid lab calibrations (Fig. 1C). Pure sulfuric

413 acid shows a large deviation from the pure AS triangle point (similar to increasing AN_f), nearly

414 doubling the values for the $nfH_ySO_x^+$ ions. This implies that a particle containing sulfuric acid

415 would produce a strong negative bias on the estimate of OS by the Chen method.

3.2 Evaluation of the Chen Method with Aircraft Field studies

The results of applying the Chen et al. (2019) method to five aircraft campaigns are shown in Fig. 1. The effect of internally mixed ammonium nitrate (AN) was explored in Fig. 1A and Sect. 3.1 (for laboratory studies). Here we explore the effect for field data from KORUS-AQ (near Seoul, South Korea) where AN was often a major aerosol component; average $AN_f \sim 0.18$). As discussed in Sect. 3.1, as the percent of AN in laboratory mixtures of AS/AN increases, so do the $nfH_ySO_x^+$, ions. The same effect is observed for the KORUS-AQ campaign, although the departure from the AS vertex is observed at substantially lower AN fractions for the field data ($AN_f \sim 0.30$). When field data is affected by AN, the Chen method might be applicable for situations with $AN_f < 0.30$. At higher fractions, a correction could potentially be developed, but with increased resulting uncertainty.

The effect of OA (shown in Fig. 1B for laboratory data) on sulfate fragmentation in ambient data is less clear due to the lack of data that has a lower AN_f, higher pH, and little/no OS (see Table S1 for average campaign OA_f). In the presence of any one of those factors, the sulfate fragmentation will be affected. It is especially challenging to confirm the absence of OS, due to the lack of direct total OS measurements available. In Fig. S7, we isolate a subset of the KORUS-AQ dataset (where $AN_f < 0.3$ and pH>0, defined as "regime II" and discussed in detail in Sect. 3.4) to see if there is an offset in the AS under these chemical conditions as observed in the laboratory data shown in Fig. 1B. Similarly to the lab data, there appears to be a ~10% offset between the pure AS $fH_ySO_x^+$ values from calibrations, and the KORUS-AQ data that occupies regime II (average $OA_f \sim 43\%$). This offset is smaller than some of the offsets observed in the

437 laboratory data (Fig. 1B and S6), but may hinder the ability of the Chen OS_f quantification

438 method to estimate [OS] even in conditions where the pH>0 and the AN_f<0.3.

439   In Fig. 1D, average values for each campaign in regime I, defined as AN_f < 0.3 and

440 calculated pH > 0, are shown. For less acidic aerosols/conditions and in the absence of OS or

441 AN_f effects, it is expected that the data would fall on top of the [1,1] pure AS point in the 1D

442 triangle plot, but this is not observed. This shift suggests that there are other factors (such as the

443 presence of organics) that affect the location of the pure AS point. In addition, the average values

444 for the different campaigns vary substantially, so it is unlikely that a "corrected" pure AS point

445 can be used for all campaign and/or lab data.

446   To further look into the potential effect of acidity, we consider the ATom campaigns in

447 Fig. 1C. ATom focused on remote oceanic air, with very low AN_f (< 0.01). This is expected as

448 AN is semivolatile (DeCarlo et al., 2008; Hennigan et al., 2008; Nault et al., 2018) and for the

449 very low calculated pH conditions during ATom (~ -1 to 1, average of -0.6), most of the nitrate

450 will be in the form of HNO_3(g) (Guo et al., 2016). The PALMS instrument independently reports

451 OS_f ~ 0.3 - 0.7% for ATom (depending on the pH). The results for ATom span the range between

452 pure AS and pure H_2SO_4, following a monotonic trend as acidity increases, consistent with the

453 laboratory results and the results from the WINTER campaign in Chen et al. (2019). We

454 hypothesize that high acidity is leading to the observed departure from the Chen triangle. Hence,

455 the ATom results suggest that all of the sulfate sampled is inorganic and if the Chen method is

456 applied OS_f = -26% to +4%. Thus the Chen method is insufficient to describe the trends

457 observed for very acidic aerosols, until calculated pH increases to ~ 0 (where the ATom data

starts to converge onto the pure AS data point). For campaigns containing particles of calculated pH > 0, the Chen method might be applicable.

To further illustrate that the ATom and KORUS-AQ campaigns are representative of the range of airmasses in the troposphere, Fig. 1D shows results for two additional campaigns that focused on the continental US. SEAC[4]RS and WINTER represent chemical regimes that are not extremely acidic (average calculated pH SEAC[4]RS ~ -0.2, WINTER calculated pH ~ 1.2). SEAC[4]RS had low AN_f (~ 0.04), while WINTER had high AN_f (~ 0.25). It is observed that every single campaign average falls outside of the triangle (for the full campaign and non-acidic, low AN_f averages), indicating that the Chen et al.(2019) method, as proposed, is not applicable to many regions of the atmosphere. Average AN_f, OA_f, and calculated pH values for different campaigns are shown in table S1.

3.3 Physical Interpretation of the Sulfate Fragmentation Trends

We note that this section (3.3) should be of most interest for AMS/ACSM users, and can probably be skipped by others. It is useful to provide a physical interpretation of the trends that are likely driving the observed sulfate fragmentation changes, based on the physicochemical details of the AMS detection and those of the particles being sampled. In Fig. 2A, a simplified diagram of the AMS detection process is shown, highlighting important details that are thought to give rise to the observed trends.

Ambient particles containing AS, OS, and other species are sampled into the AMS through a focusing lens. Following a series of differential pumping steps through the instrument, the particles impact on a porous tungsten standard vaporizer. The time spent under vacuum from

479 sampling to detection is of the order of 15 ms. A fraction of the more viscous particles may

480 bounce from the vaporizer without detection. Non-refractory species in the particles that stick to

481 the vaporizer (such as OS and AS) are heated by heat transfer from the vaporizer surface. Some

482 species may evaporate in the form in which they are present in the particle, while others may

483 thermally decompose to other species, which then evaporate. For example, ammonium sulfate

484 may evaporate to $H_2SO_4(g)$ and $NH_3(g)$, but it may also thermally decompose to $SO_2(g)$, $SO_3(g)$

485 and $H_2O(g)$ (Hu et al., 2017b). Finally, these gaseous thermal decomposition products undergo

486 electron ionization to become positively charged species. Since the electrons used in EI have far

487 more energy (70 eV) than typical bonds in a molecule (~6 eV for S=O), the initial ions may

488 fragment into smaller ions if the ionization process results in absorption of > 6 eV of internal

489 energy by the molecule, beyond the ionization energy (Lambert, 1998). Some of the evaporated

490 $H_2SO_4(g)$ may remain as $H_2SO_4^+$ after ionization, or it may fragment to HSO_3^+ or SO_x^+ ions.

491 $SO_2(g)$ can only produce SO_x^+ ions. Thus the mixture of fragments observed will retain some

492 memory of the species that evaporated from the particles. If the mixture of evaporating species is

493 influenced by the particle composition (e.g. pH, AN, OA, or OS_f) then it may be possible to

494 calibrate the observed relationship to estimate a particle intensive chemical property.

495   Fig. 2A also shows a schematic close-up of the SV surface, which is the main point in the

496 instrument that controls ammonium sulfate fragmentation. In this diagram, we show a

497 non-smooth surface with pores, consistent with the fabrication of the vaporizer by sintering 50

498 μm tungsten spheres. The interaction of a particle with this porous surface is dependent on the

499 particle phase / viscosity. The red particles represent rigid (more solid-like) particles. These rigid

500 particles can simply bounce off of the vaporizer, leading to no detection. AS-dominated particles

are likely to be rigid (due to the solid phase of pure AS), thus increasing bounce and lowering the

AMS CE (Matthew et al., 2008; Middlebrook et al., 2012). AS particles can also become trapped

in the porous surface. When trapped, they are heated by conduction from the vaporizer surface

and by radiation from surrounding surfaces. They reach higher temperatures that lead to more

thermal decomposition, and a lower $H_2SO_4(g)/SO_x(g)$ ratio. Consistent with this interpretation, it

was shown that the $H_2SO_4^+/SO^+$ fragment ratio increased as the vaporizer temperature was

reduced while sampling ambient air, while the SO_2^+/SO^+ ratio did not change (Docherty et al.

(2015), their figure S5). In addition, molecules that evaporate as $H_2SO_4(g)$ from these trapped

particles are likely to collide with tungsten surfaces on their way out to the ionization region,

leading to additional thermal decomposition (Hu et al., 2017b) and further reducing the

$H_2SO_4(g)/SO_x(g)$ ratio for the gases reaching the EI region, and thus the $H_ySO_x^+/SO_x^+$ ion ratio.

The second case (blue particle) represents the situation where the particle is less

rigid/viscous or liquid. Acidic sulfate particles (with a lower fraction of the sulfate ions

neutralized by NH_4^+), particles with high AN_f, or particles coated with a large water or liquid

organic layer are more likely to deform upon impact and not bounce. This leads to an increased

CE (Matthew et al., 2008; Middlebrook et al., 2012; Hu et al., 2017a). There are several effects

that will lead to a higher $H_2SO_4(g)/SO_x(g)$ ratio reaching the ionization region in this situation:

(a) evaporated $H_2SO_4(g)$ from particles that impact the front of the vaporizer and do not bounce

can now escape without further collisions with the tungsten surface; (b) the increased surface

area from impact deformation and the lower viscosity allow more $H_2SO_4(g)$ molecules to escape

the particle before those molecules are heated to temperatures that would lead to thermal

decomposition.

523 In Fig. 2B, we show a conceptual model of the impact of these phenomena on the Chen

524 triangle. For very acidic sulfate (approx. a calculated pH < 0), the liquid character of the

525 particles leads to less bounce in the vaporizer. It also leads to faster evaporation, which reduces

526 the internal temperature for the particles and that of the evaporated molecules, leading to less

527 fragmentation. In this part of the atmosphere, OS_f cannot be estimated, but pH may be, as long as

528 it can be assumed (or shown by additional measurements from the AMS or other instruments)

529 that OS_f and non-volatile cations are small. As an air mass becomes more neutralized by NH_4^+,

530 the particles become less acidic and more rigid/viscous, leading to more thermal decomposition

531 of the evaporated species, and the fragmentation of ammonium sulfate occurs at the upper vertex

532 of the triangle. In this part of the atmosphere, methods such as Chen et al. (2019) may be

533 applicable to estimate OS_f, as long as there are no other effects that interfere with the sulfate

534 fragments detected (such as substantial non-volatile cations or variations in possible OA effects).

535 As more ammonia is added to an airmass, the acidity of the particles decreases and the higher pH

536 favors the partitioning of $HNO_3(g)$ to the particle phase, forming ammonium nitrate. If AN_f

537 becomes high enough (> 0.3), the particles again become less rigid/viscous and the

538 fragmentation shifts again outside the Chen triangle for the same reasons discussed for the acidic

539 particles. Finally, Fig. 2C shows the differences in the detection process and the fragments

540 produced in the AMS for OS and/or AS/H_2SO_4.

541 **3.4 Specification of aerosol chemical regimes for feasibility of OS_f quantification**

542   In Fig. 3A, we introduce a plot of AN_f vs. calculated pH that can be used to evaluate the

543 applicability of the OS_f methods to different datasets. Data for five different campaigns (those

544 with AS calibrations, labelled "C" in Table 1) are shown, along with the campaign averages.

545 Regime I ("highly acidic, low AN") occupies the bottom left quadrant, where $AN_f < 0.3$ and

546 calculated pH < 0. Campaigns sampling the more remote atmosphere (e.g. ATom-1, 89% of

547 datapoints; ATom-2, 80%), and a fraction of the data from continental campaigns (SEAC^{4}RS,

548 13% ; DC3 , 40%) fall in this regime. For remote regions, emissions (such as NH_3 and NO_x) are

549 generally low. Remote oceanic regions are relatively isolated from the major continental

550 ammonia sources (Paulot et al., 2015). Therefore, less ammonia is available to balance the

551 hydronium ions from H_2SO_4, leading to high acidity (Quinn et al., 1988; Keene, 2002; Nault et

552 al., 2020). Highly acidic aerosols and lack of NH_3 shift HNO_3 to the gas phase, so low AN_f is

553 observed. In contrast, for sampling in polluted source regions with strong HNO_3 formation and

554 substantial NH_3 emissions, a much smaller fraction of the data falls in this regime (e.g. only 4%

555 for KORUS-AQ). In Sect. 3.5 we discuss the potential to estimate pH from AMS data in regime

556 I.

557   Regime II (lower right) involves less acidic conditions (calculated pH > 0) and lower AN_f

558 (< 0.3). In this region sulfate fragmentation in the AMS is not strongly impacted by either AN_f or

559 acidity. In principle, in this regime the recently proposed sulfate deconvolution methods could be

560 applicable. The geographical regions studied in Chen et al. (2019) and Song et al. (2019)

561 generally fall in this regime, and this might explain the lack of large negative OS_f values in those

562 studies, in contrast to our observations for other regions. About half of our campaign data is

563 located in this regime, more so for the continental campaigns and much less so for the remote

564 campaigns. Specifically, 65% of KORUS-AQ, 60% of DC3, 87% of SEAC^{4}RS, 11% of ATom-1

565 and 20% of ATom-2 fall in this regime. We have applied the 1D version of the Chen method to

566 each field campaign after filtering it by the AN_f and calculated pH constraints for regime II. OS_f

567 is nominally slightly greater than zero for ATom-1, $OS_f \sim 3\%$, of the order of the 0.3% estimate

568 in regime II from PALMS (for ATom-1 and ATom-2, estimated by only considering the sulfate

569 moiety from the IEPOX or glycolic acid sulfate (GAS) OS, neither of which was detected in the

570 supermicron aerosol (Froyd et al., 2009, 2019; Liao et al., 2015) (see Fig. S8). However, OS_f is

571 much less than zero for ATom-2 ($OS_f \sim$ -23%) and KORUS-AQ ($OS_f \sim$ -26%). These

572 unreasonable results may be due to the effect of OA on sulfate fragmentation in the AMS

573 (discussed in Sect. 3.2). For this reason, strong caution is advised in applying OS_f estimation

574 methods to ambient data, even in regime II. In addition, estimating OS with sulfate ions may be

575 susceptible to errors due to inaccuracies in AS calibrations, noise present in the ambient data, or

576 other factors.

577   We also show results from applying the Song et al. (2019) method in regime II (which is

578 based on similar principles to the Chen method) in Fig. S9. Similarly to the Chen method, we see

579 that most OS_f values are predicted to be less than zero. For the entire atmosphere, shown in Fig.

580 S10, the distribution for OS_f looks similar to Fig. S9.

581   Regime III is characterized by high AN_f (> 0.3) and lower acidity (calculated pH > 0).

582 This chemical regime primarily exists in polluted continental regions near large source regions

583 such as megacities and agricultural regions, as high NO_x and NH_3 emissions can lead to

584 increased particulate AN and an increase in aerosol pH (Pye et al., 2019). In this regime, there

585 are strong variations in the AMS sulfate fragments that are driven by AN_f. OS_f cannot be

586 estimated with the AMS sulfate fragmentation methods proposed so far, unless they are further

587 modified to account for the AN_f effect. ~ 31% of KORUS-AQ data falls in this regime, but

588 almost none of the data from the rural / remote campaigns falls in this region, as AN typically

589 evaporates as the air is diluted during advection away from polluted regions (DeCarlo et al.,

590 2008).

591   Finally, regime IV in the top left quadrant has high AN ($AN_f > 0.3$) and high acidity

592 (calculated pH < 0). This chemical regime is unlikely to be observed in the real atmosphere, and

593 indeed there are very few points in that region for our campaigns. Sulfate is ubiquitous (Zhang et

594 al., 2007b; Hodzic et al., 2020), and nitrate is not thermodynamically stable in the aerosol phase

595 together with acidic sulfate for calculated pH < 0 (Guo et. al., 2016). For all campaigns we

596 observe ~ 0% of points occupying this regime. Very unusual datapoints can be observed when

597 ammonium nitrate-containing particles are externally mixed with acidic sulfate containing

598 particles in an airmass.

599   Since the field studies analyzed here targeted large regions but did not sample many

600 others, it is of interest to evaluate the fraction of the troposphere located in each one of the

601 chemical regimes. The results of the GEOS-Chem v12 model are used for this purpose in Fig. 3B

602 and shown as a global map in Fig. 4 and Fig. S11. ~ 67% of the model troposphere exists in

603 regime I (calculated pH < 0). In addition, ~ 33% of the global troposphere exists in regime II

604 where it may be feasible to estimate OS_f from AMS fragments. Less than 1% of the modeled

605 atmosphere exists in regime III (upper right quadrant) where ammonium nitrate strongly

606 influences sulfate fragmentation, consistent with the relatively small very polluted geographical

607 regions with very large AN_f. Finally, none of the data fell in regime IV, consistent with aerosols

608 being assumed to be internally mixed in GEOS-Chem. At the surface during December, January,

609 and February (DJF) (Fig. 4A), most of the remote oceans fall in regime I (calculated pH < 0 and

610 $AN_f < 0.3$), while regime II (calculated pH > 0 and $AN_f < 0.3$) is dominant over continental

611 regions. At the surface in June, July, and August (JJA) (Fig. 4C), most of the globe is in regime

612 II. Very little of the data falls in regime III, except parts of Asia, regardless of season. A similar

613 pattern is observed in the free troposphere (Fig. 4B and 4D) with some geographical differences.

614 Regime III (calculated pH > 0 and $AN_f > 0.3$), which represents pollution hotspots, is observed in

615 a large region in Asia during the Summer months, whereas the Winter months are dominated by

616 regime I (low pH). The Summer months in the free troposphere are also mostly in regime II,

617 especially over continental regions. Due to averaging of an entire year, as well as the limited

618 spatial resolution of the GEOS-Chem model, locations and periods of high AN_f hotspots are not

619 as prominent in these results, even when the data are divided by season.

620 **3.5 Potential pH estimation from AMS measurements**

621 **3.5.1 Estimation of pH from AMS sulfate fragments**

622   In Sect. 3.4, we introduced chemical regime I with low calculated pH and low AN_f. In

623 this regime, which encompasses about half of the campaign data and ⅔ of the modeled global

624 troposphere, PALMS data shows that the overwhelming majority of the sulfate is inorganic, with

625 OS_f contributing ~ 0.7% to total sulfate by mass during ATom-1 and ATom-2 when calculated pH

626 < 0 (see Fig. S8, in regime I). This removes sulfate fragmentation changes caused by AN and

627 sulfate type (OS vs. AS), indicating that sulfate fragmentation is almost exclusively controlled by

628 the acidity of the aerosol. Fig. 1C shows that $fH_2SO_4^+$ and $fHSO_3^+$, i.e. the amount of sulfate

629 fragments retaining one or two hydrogens ($H_2SO_4^+$ and HSO_3^+) relative to the total sulfate

630 fragments ($H_2SO_4^+$, HSO_3^+, SO_3^+, SO_2^+, and SO^+) increases as calculated pH decreases.

631   In Fig. 5 we show the relationship between $H_ySO_x^+/SO_x^+$ and aerosol pH. As the

632 relationship is noisy for individual data points, we show the results for 5% quantiles of the data.

633 $H_ySO_x^+/SO_x^+$ appears to show a proportional relationship with decreasing calculated pH for the

634 ATom campaigns, for which much of the data is in regime I. The KORUS-AQ data, of which

635 very little falls in the regime I, does not show a relationship between these variables, as expected.

636 A fitted equation to the ATom relationship may allow the real-time estimation of pH for different

637 air masses for campaigns in regime I as:

$$pH = -1.3\,(\pm 0.06) + 6.0(\pm 1.2) \times e^{-1.3(\pm 0.18)\times \frac{H_ySO_x^+}{SO_x^+}}$$ Eq. 13

638 As shown in the histogram in Fig. 5B, this relationship is applicable to a substantial fraction of

639 ambient observations. This estimation equation likely needs to be calibrated for each instrument

640 (e.g. by sampling sulfate particles with different acidities), since the sulfate fragmentation does

641 vary with instrument (Chen et al., 2019) and potentially also in time for a given instrument.

642   Although an estimation equation that apparently works for only one unit of pH may seem

643 of limited value, two caveats apply: first, it is of high value to know that the estimated pH < 0 for

644 a certain air mass (as opposed to e.g. estimated pH = 2 or 3 that are frequently encountered).

645 Second, the range of estimated pH below 0 is limited here due to not considering the activity

646 coefficient. If that coefficient was included, the predicted estimated pH range in this regime

647 would be ~ -4 to 0.

648 **3.5.2 Estimation of pH from Ammonium Balance**

649   Ammonium balance (NH_{4_bal}) (Eq. (7)) is often used as a qualitative indicator of acidity.

650 (Zhang et al., 2007a) showed that calculated pH under constant temperature and RH was well

651 correlated with ammonium balance, but much more scatter was observed when the instantaneous

652 T and RH were used. Several studies have argued that ammonium balance cannot be used to

653 estimate ambient pH (e.g., Guo et al., 2015, 2016; Hennigan et al., 2015; Weber et al., 2016);

654 however, those studies were all performed at continental ground sites that were in the less-acidic

655 chemical regimes (II and III), and where daily temperature and humidity changes were strong.

656 As shown in Fig. 6, NH_{4_bal} and calculated pH for the aircraft studies show a strong and

657 consistent relationship in regime I (calculated pH < 0), providing another potential method for

658 estimating pH (all one needs to use this method is the ammonium balance, and if it is < 0.65, the

659 method should be applicable). As ammonium balance increases, so does calculated pH across the

660 six campaigns studied. These data are generally outside of the continental boundary layer, where

661 temperature and RH change less in a diurnal cycle, reducing the impact of those changes on pH.

662 For data in regimes II-III (calculated pH > 0) some proportionality of pH and NH_{4_bal} is still

663 observed on average, but with more dispersion across campaigns. Given the similarity of the

664 results for regime I, the fitting equation of calculated pH vs. ammonium balance may be used to

665 provide a near real-time estimate of pH (for NH_{4_bal} < 0.65).

$$pH = -1.1(\pm 0.031) + 1.7(\pm 0.089) * NH_{4\_bal} \qquad \text{Eq. 14}$$

666 As shown in the histogram in Fig 6B-6D, this relationship is also applicable to a

667 substantial fraction of ambient regions. This estimation equation should be tested with other

668 studies. An advantage of this relationship (vs. the one based on $H_ySO_x^+/SO_x^+$) is that it is likely to

669 be less instrument-dependent, as long as careful calibrations of RIE_{NH4} and RIE_{SO4} have been

670 performed. Conditions where non-volatile cations (e.g. Na^+, K^+, Ca^{2+}) are important for

671 submicron particles could lead to deviations from this relationship (Guo et al., 2020). However,

672 such conditions are infrequent in remote air (Nault et al., 2020) and can be diagnosed by

673 concurrent supermicron or filter measurements.

674 **3.5.3 Application of pH estimation methods to ambient data**

675 As discussed above, ammonium balance and $H_ySO_x^+/SO_x^+$ are two measurements that

676 may be used to estimate aerosol acidity in parts of the atmosphere. In Fig. 7 these two methods

677 are applied to one flight during ATom-1 and an SO_2 plume sampled during WINTER. In Fig. 7A,

678 both $H_ySO_x^+/SO_x^+$ and NH_{4_bal} follow the trend for E-AIM calculated pH during most periods

679 when calculated pH < 0, even at one minute time resolution.

680 As expected from Fig. 6, NH_{4_bal} is a less noisy, more robust metric for estimating pH at

681 one minute time resolution. Unlike $H_ySO_x^+/SO_x^+$, NH_{4_bal} appears to be able to capture basic

682 calculated pH trends at the full range of calculated pH values observed during this flight in

683 ATom-1. NH_{4_bal} also matches the E-AIM calculated pH well for the WINTER power plant

684 plume. For RF01 in ATom-1 (WINTER), NH_{4_bal} estimated pH has an $R^2 \sim 0.6$ (0.9) for pH<0

685 (Fig. 7C-D).This shows that in the remote atmosphere (like in ATom) or in an SO_2 plume, NH_{4_bal}

686 has the potential to allow fast estimation of pH, even under relatively low sulfate concentrations,

687 albeit not perfectly. More scatter is observed for the estimate based on $H_ySO_x^+/SO_x^+$, indicating

688 that longer averages are needed for this method. The error is typically within +/- 0.5 estimated

689 pH units, which is thought to be the accuracy of thermodynamic pH estimation models.

690 **3.6 Possibility of Estimating Collection Efficiency (CE) from Sulfate Fragmentation**

691   From the previous discussion it is clear that sulfate fragmentation changes due to some of

692 the same factors (acidity, AN_f) that influence ambient AMS CE. It is of interest to explore

693 whether a quantitative estimate of ambient particle CE could be derived from the measured

694 sulfate fragments, at least under some conditions, as it could provide a complementary

695 characterization to the CE estimates from the Middlebrook et al. (2012) parameterization. In Fig.

696 8 we show the CE estimated from Middlebrook et al. (2012) vs. $H_ySO_x^+/SO_x^+$ for ATom and

697 KORUS-AQ. CE does show some relationship with $H_ySO_x^+/SO_x^+$, with most sensitivity around

698 CE ~ 0.8-0.9. A substantial level of noise is observed on the high-time resolution data, and the

699 trend varies between the two campaigns (where variations in CE are controlled by two different

700 effects, acidity vs AN_f). Further research would be necessary to evaluate whether this method

701 could be used to estimate CE.

Conclusions

703   The presence of organosulfates in particles is a topic of much recent interest, but there is

704 a lack of online methods to quantify them. Two methods have been proposed to use widely

705 available AMS data to quantify OS_f (Chen et al., 2019; Song et al., 2019). These methods have

706 only been applied to ground continental datasets, to our knowledge. We show using both

707 laboratory and field data that both high acidity (regime I) and high AN_f (regime III) result in

708 major changes in sulfate fragmentation, which often lead to nonsensical results for the OS_f

709 methods. Regime I accounts for ~ ⅔ of the global troposphere , while regime III can be

710 important in polluted regions (e.g. Seoul region), and thus it is critical to avoid applying the

711 proposed OS_f estimation methods in these regimes. In regime II, with lower acidity and lower

712 nitrate (calculated pH > 0, AN_f < 0.3) OS_f estimation methods may be applicable, if no other

713 effects (e.g. significant non-volatile cations or variations in OA effects) confound the sulfate

714 fragmentation. For the ambient data analyzed here, even in regime II the OS_f estimation

715 produced nonsensical results. Extreme caution is recommended to anyone who chooses to apply

716 the OS_f estimation methods. For reasons not fully understood, fragmentation of the sulfate ions

717 in the lab vs. ambient data differ at times.

718   We investigated two different methods to estimate pH in real-time in regime I (calculated

719 pH < 0 and AN_f < 0.3), based on the AMS $H_ySO_x^+/SO_x^+$ fragment ratio and the ammonium

720 balance, respectively, without the need to run a thermodynamic model, and without the need for

721 gas-phase NH_3 or HNO_3 measurements. Low OS_f and non-volatile cations need to be assumed or

722 confirmed from AMS and other measurements. The ammonium balance method shows better

723 performance. These *in-situ* and direct pH estimation methods should be applicable in the remote

724 atmosphere (oceanic regions, and often the continental free troposphere when not recently

725 impacted by surface sources). Both the OS_f and pH estimations require careful instrument

726 calibration for a given campaign, and the methods based on sulfate fragments are expected to be

727 instrument-dependent, including for the same instrument in time when filaments or the vaporizer

728 are replaced, or when the instrument is re-tuned. Both methods should be further evaluated with

729 data from other studies.

730   We propose a conceptual model to explain the observed sulfate fragmentation changes

731 with changing particle chemical composition. As particles become more acidic or higher in AN,

732 a higher fraction of $H_2SO_4(g)$ can reach the ionization region, leading to changes in the observed

733 ion population. Since AMS CE is thought to be controlled by the same effects, we explore

734 whether it can be estimated from the observed sulfate fragmentation, and find that while changes

735 in $H_ySO_x^+/SO_x^+$ do correlate to changes in CE, the relationship is not the same across different

736 campaigns. Further investigation of this relationship, especially when direct CE measurements

737 are available via internal AMS light scattering, would be of interest.

738 We have not explored the application of these methods to ACSM data. ACSM data are

739 unit-mass resolution, and the interferences between species at a given unit mass are estimated

740 using a fragmentation table approach (Allan et al., 2004). This approach introduces more

741 uncertainties, as exemplified by Hu et al. (2015) for similar fragment-based methods.

Data Availability

755 DC3 data available at DOI: 10.5067/Aircraft/DC3/DC8/Aerosol-TraceGas, last accessed on 9
756 September, 2018. SEAC⁴RS data available at
757 http://doi.org/10.5067/Aircraft/SEAC4RS/Aerosol-TraceGas-Cloud, last accessed on 27 April,
758 2020. WINTER data available at https://data.eol.ucar.edu/master_lists/generated/winter/, last
759 accessed 27 April 2020. KORUS-AQ data available at DOI:
760 10.5067/Suborbital/KORUSAQ/DATA01, last accessed 14 June, 2018. ATom-1 and ATom-2
761 data available at https://doi.org/10.3334/ORNLDAAC/158, last accessed 27 April 2020.

Tables and Figures

Table 1. Summary of the campaigns used in this study. See SI Fig. S1 for flight paths. Reference
label refers to the type of data used for each campaign throughout this paper, depending on the
quality and completeness of the data, for the purposes of a specific analysis. A : ammonium
balance, f: SO_4 campaign-averaged fragments, F: SO_4 campaign-average and time-resolved
fragments , and C: pure AS calibration data reliable and used.

| Campaign	Location	Season/Year	References	Reference Label
DC3: Deep Convective Clouds and Chemistry	Mid-Latitude Continental United States	Spring/Summer 2012	Barth et al., (2015)	A
SEAC⁴RS: Studies of Emissions and Atmospheric Composition, Clouds and Climate Coupling by Regional Surveys	Continental United States	Summer 2013	Wagner et al., (2015); Toon et al., (2016)	A, f, C
WINTER: Wintertime Investigation of Transport, Emissions, and Reactivity	Eastern United States, continental and marine	Winter 2015	Jaeglé et al., (2018); Schroder et al., (2018)	A, f, C
KORUS-AQ: Korean United States Air Quality	South Korean Peninsula and Yellow Sea	Spring 2016	Nault et al., (2018)	A, F, C
ATom-1: Atmospheric Tomography Mission 1	Remote Pacific and Atlantic Basins	Boreal Summer/Austral Winter 2016	Brock (2019); Hodshire et al., (2019); Hodzic et al., (2020)	A, F, C
ATom-2: Atmospheric Tomography Mission 2	Remote Pacific and Atlantic Basins	Austral Summer/Boreal Winter 2017	Hodzic et al., (2020)	A, F, C
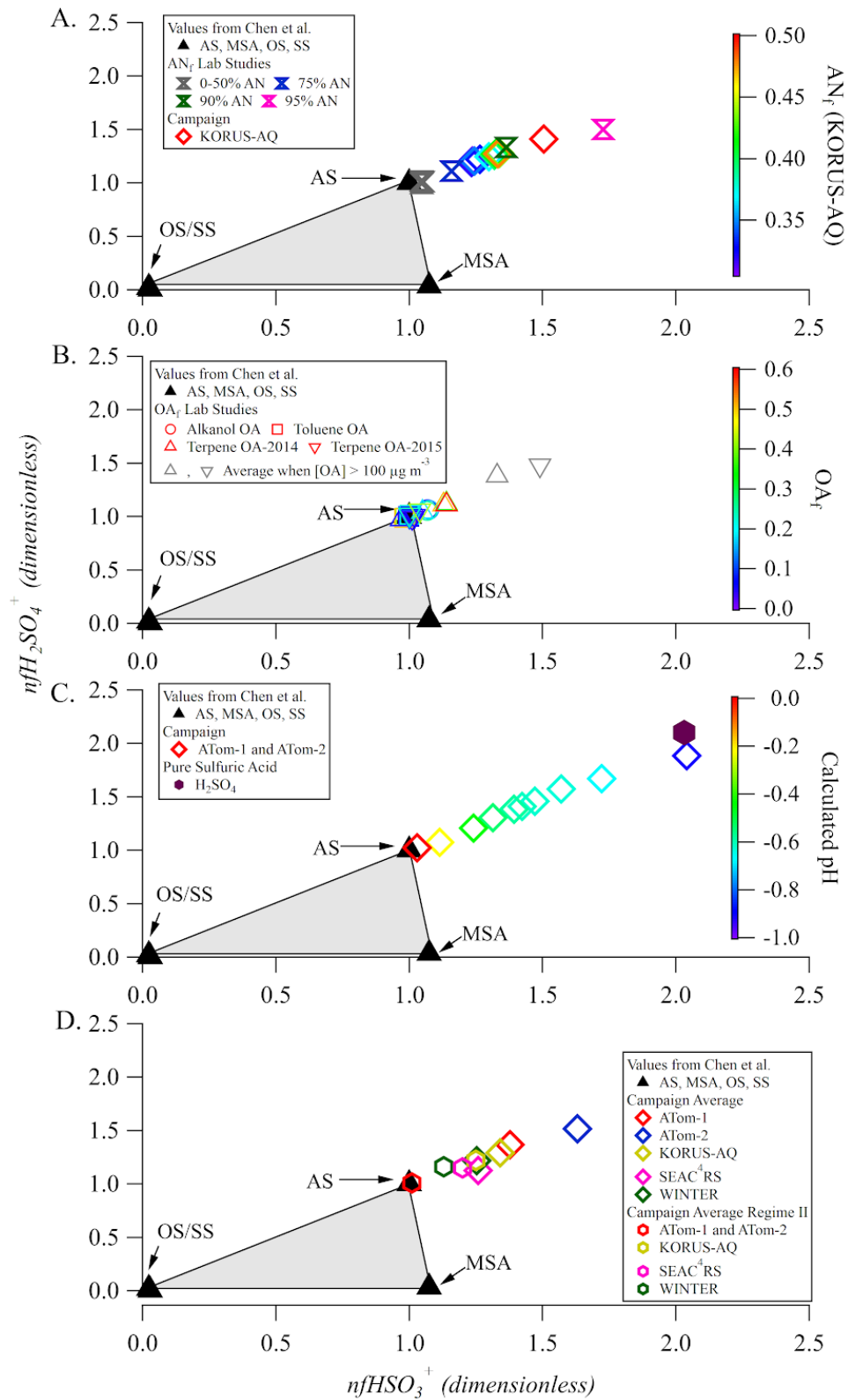
Fig. 1. Laboratory and field data for sulfate fragmentation shown in the triangle diagram proposed by Chen et al. (2019). (A) Data split into 10 quantiles of AN_f value for the full KORUS-AQ campaign, as well as for different laboratory internal mixtures of AS and AN . (B) Data from two chamber experiments, split into 5 quantiles of OA_f. Data with very high OA (>100 µg m^{-3}) are shown as grey triangles. The average of OA_f for the very high OA data in 2014 and 2015 is 0.8.Two separate datasets of monoterpene SOA chamber experiments are labelled as "2014" and "2015". (C) Data split into 10 quantiles by calculated pH for ATom-1 and 2, colored by calculated pH from E-AIM. (D) Averages for 5 aircraft campaigns for the full campaign and a subset of each campaign where pH<0 and AN_f<0.3.
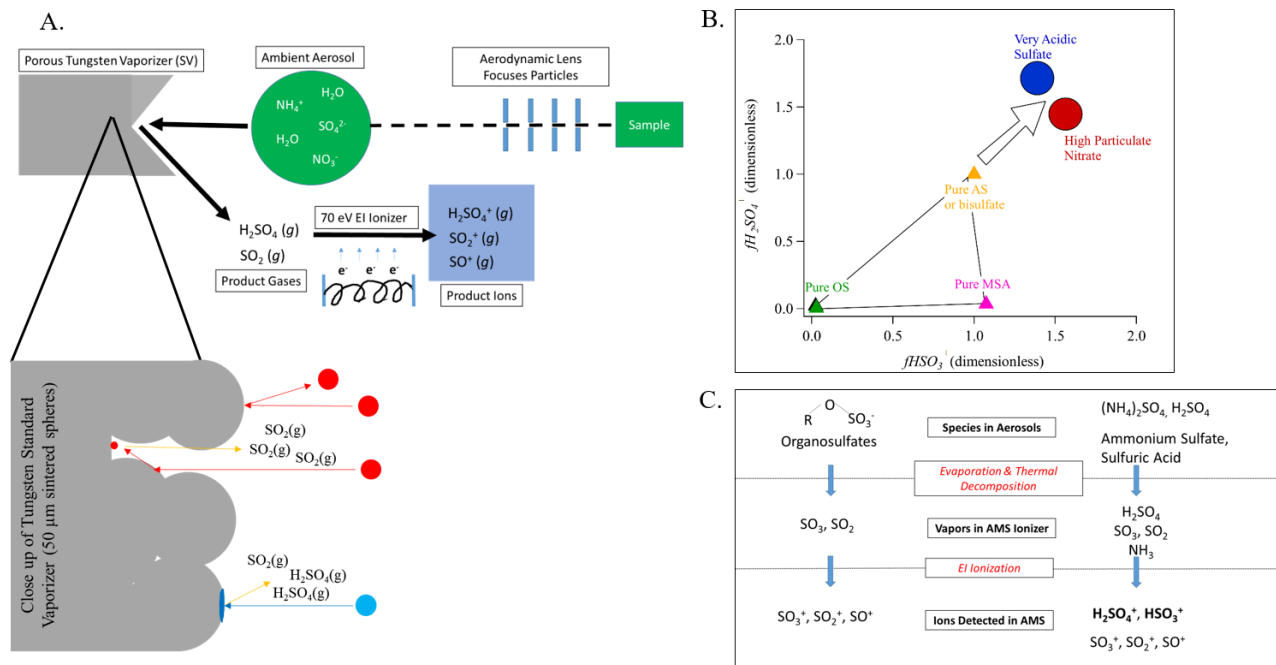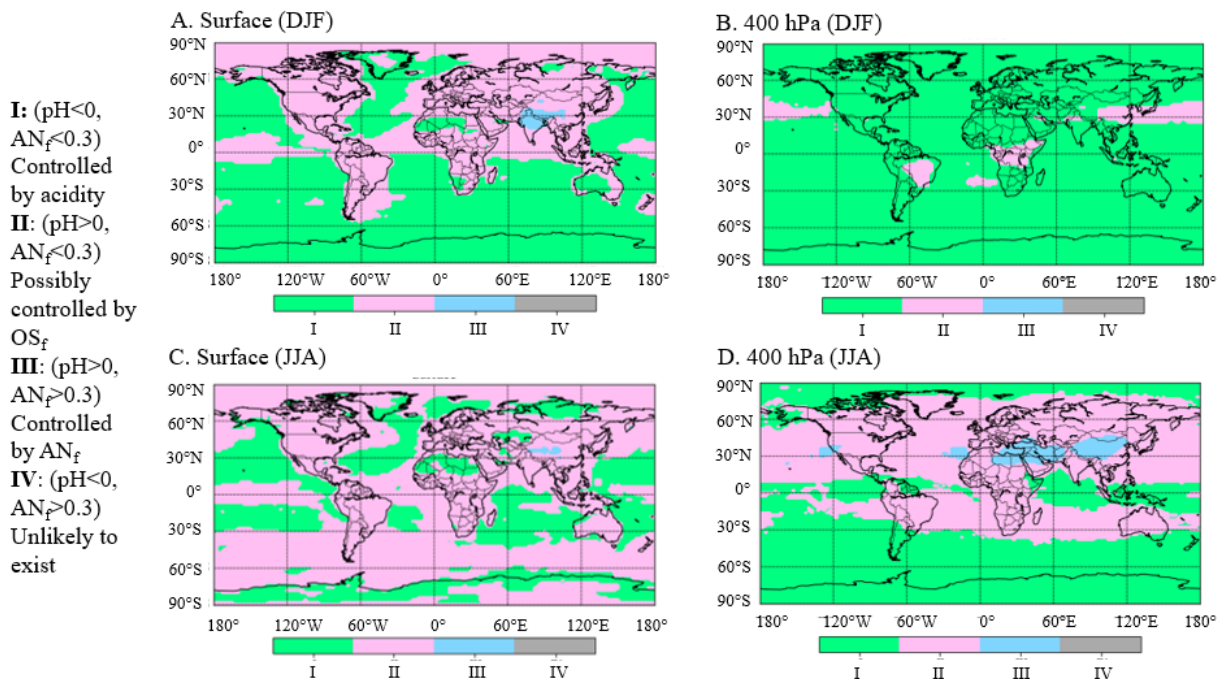
Fig. 2. (A) Simplified schematic of the AMS detection process, including a close up of the tungsten standard vaporizer surface and the different species produced by AS and OS. (B) Conceptual model of the position of particles of different compositions in the Chen et al. (2019) triangle plot. As particles become more acidic or higher in particulate nitrate, the ratio of the AMS hydrogenated to total sulfate fragments increases. When sulfate is present as AS (or mixtures of AS and ammonium bisulfate), the sulfate fragmentation is mainly impacted by OS vs. AS vs. MSA relative concentrations inside the Chen triangle. (C) Schematic of the transformations during the AMS detection process for OS and AS.
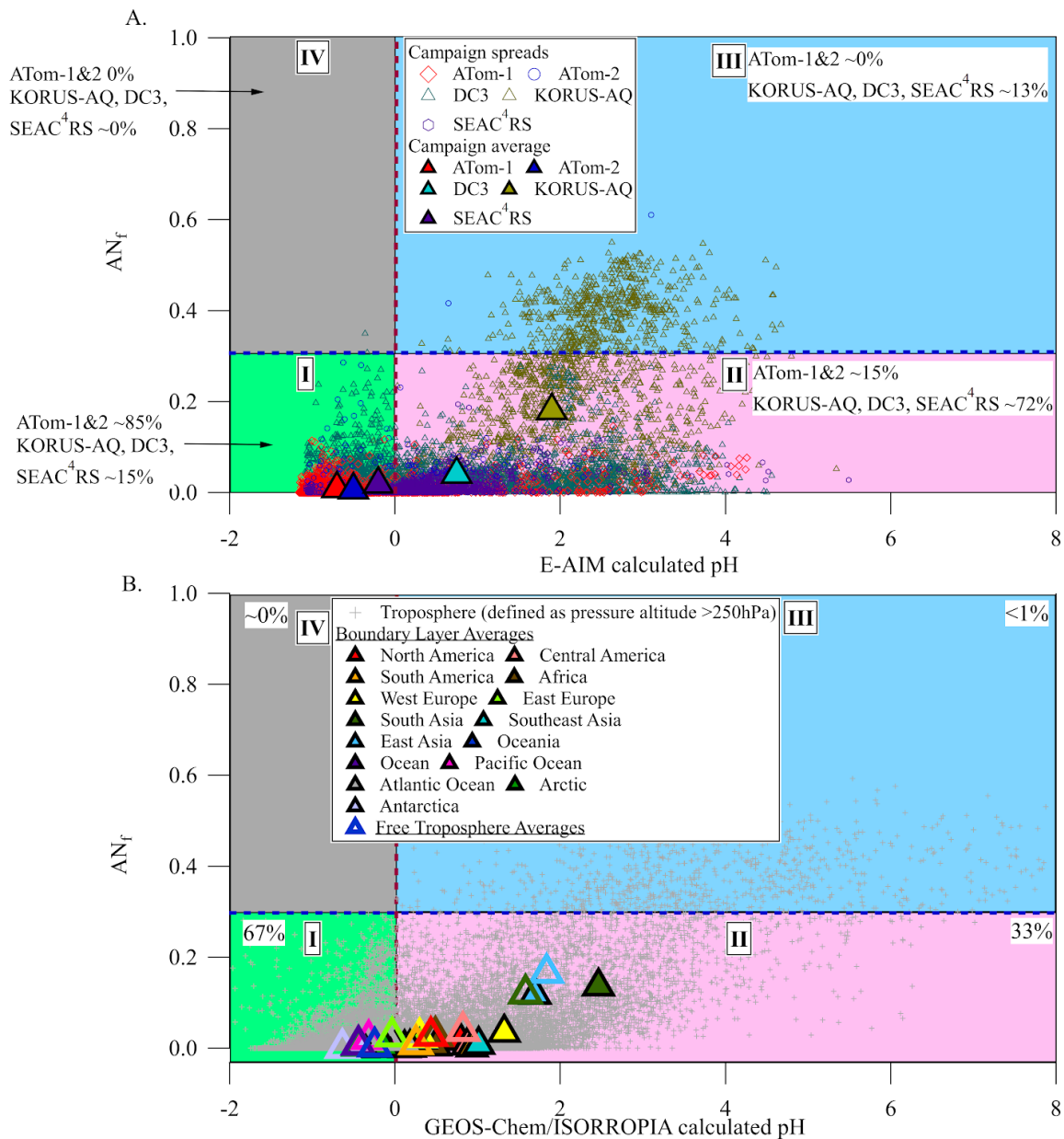
Fig. 3. (A) location of the aircraft campaign 1-minute data points on the chemical regimes defined in this paper (AN_f, from AMS measurements) vs. E-AIM pH. SEAC⁴RS, WINTER, and KORUS-AQ are averaged to one value, for brevity, but defined individually in Sect. 3.4. (B) Location of global GEOS-Chem v12 results in the chemical-regimes diagram. Yearlong averages shown as large triangles.

A. Surface (DJF)   B. 400 hPa (DJF)

I: (pH<0, AN_f<0.3) Controlled by acidity
II: (pH>0, AN_f<0.3) Possibly controlled by OS_f
III: (pH>0, AN_f>0.3) Controlled by AN_f
IV: (pH<0, AN_f>0.3) Unlikely to exist

C. Surface (JJA)   D. 400 hPa (JJA)

Fig. 4. Areas characterized by different chemical regimes according to results from GEOS-Chem v12. (A) Surface for December, January, and February (DJF), (B) 400 hPa for DJF, (C) Surface for June, July, and August (JJA), (D) 400 hPa for JJA. Roman numerals correspond to regimes in Fig. 3.
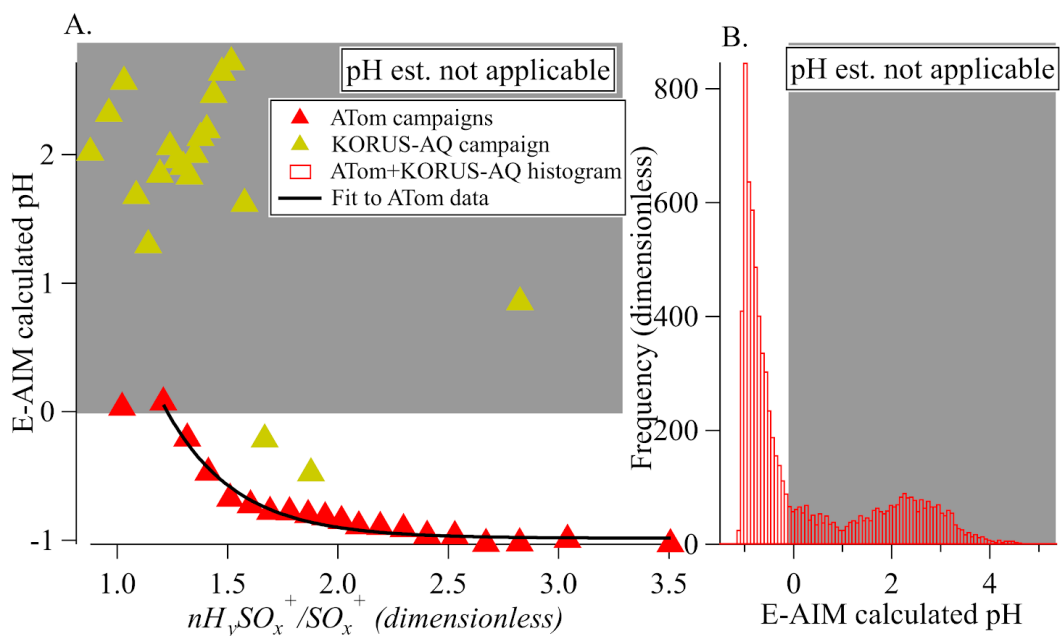
Fig. 5. (A) Calculated pH vs. sulfate fragmentation indicator ($H_ySO_x^+/SO_x^+$) for the ATom and
KORUS-AQ campaigns, and binned by $nH_ySO_x^+/SO_x^+$. The black line is an exponential fit to
ATom data (see text) when calculated pH<0. (B) histogram of the calculated pH for the 1-minute
datapoints from the ATom-1,2 and KORUS-AQ datasets. In both panels, the white (gray) area
shows the regime where calculated pH can (and cannot) be estimated from the sulfate
fragmentation.
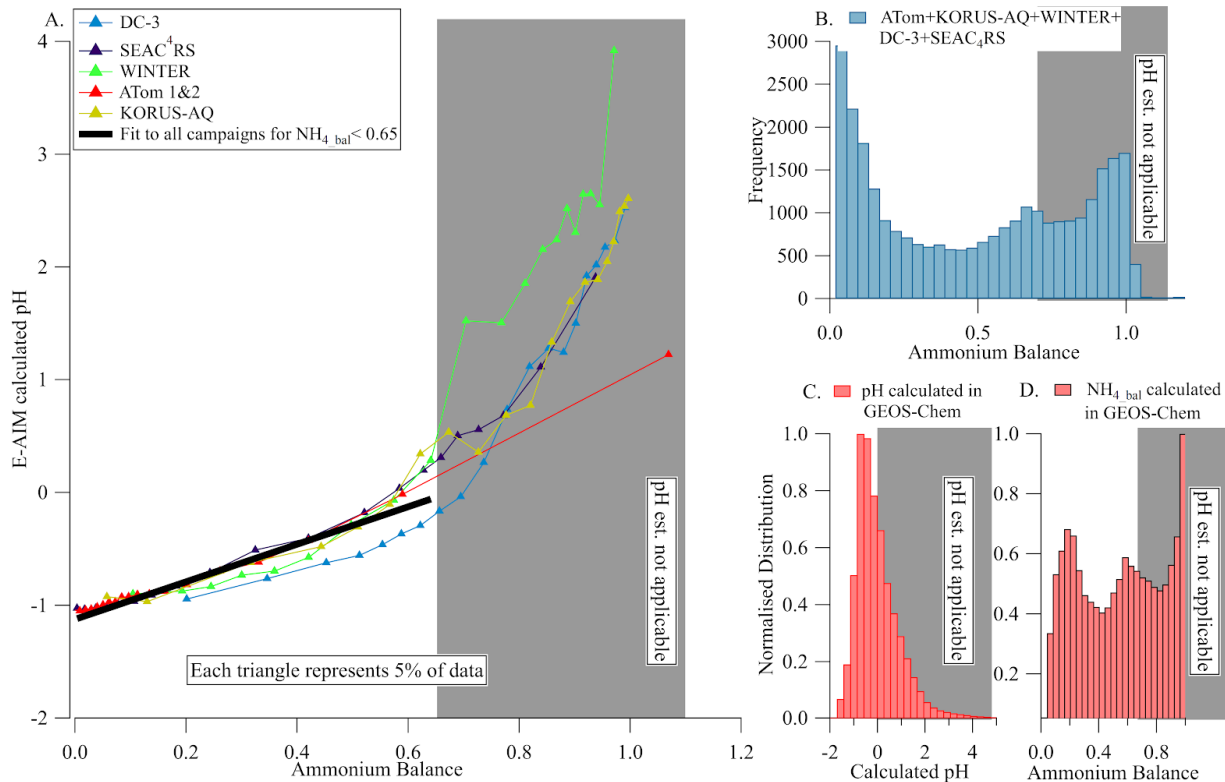
Fig. 6. (A) Calculated pH vs. ammonium balance for multiple campaigns. Quantiles of the data are used to reduce the impact of noise. The black line is an orthogonal distance regression (ODR) fit to the campaign data for values with $NH_{4\_Bal} < 0.65$. B) Histogram of measured ammonium balance for the 6 campaigns. (C) and (D), calculated pH and ammonium balance from GEOS-Chem (pH calculated with ISORROPIA). In all panels the white (grey) areas encompass the data points for which calculated pH can (and cannot) be estimated from the measured ammonium balance.
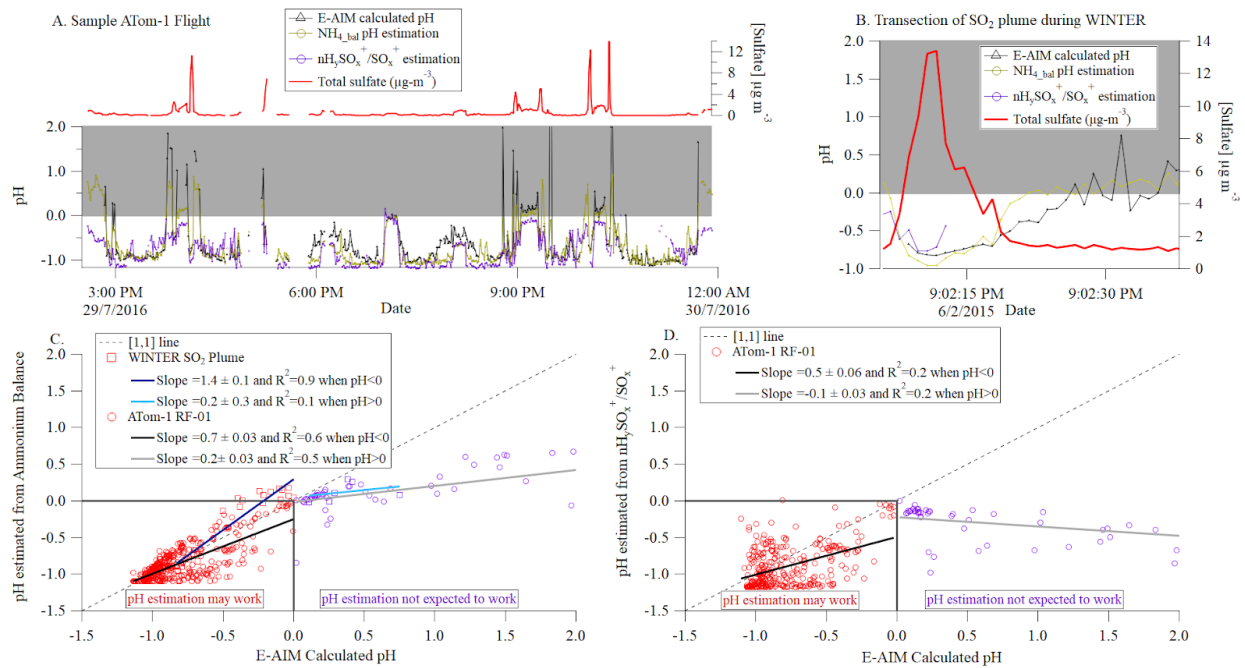
Fig. 7. (A) Time series of sulfate, pH calculated from E-AIM and estimated from $H_ySO_x^+/SO_x^+$, and NH_{4_Bal} for one flight during ATom-1 (at 1 min. resolution, filtered to remove points where sulfate was less than 3 times its detection limit). (B) Time series of sulfate and pH for a large power plant plume sampled during WINTER, only a few data points are shown for pH estimated from $nH_ySO_x^+/SO_x^+$ because sulfate in the AMS evaporated slowly during the second half of the plume transect, leading to altered sulfate fragmentation, and this effect cannot be corrected for, due to infrequent backgrounds in aircraft fast acquisition mode.(C) Scatter Plot of estimated pH predicted from NH_{4_Bal} vs. E-AIM calculated pH for the data above. (D) Scatterplot of estimated pH predicted from $nH_ySO_x^+/SO_x^+$ vs. E-AIM calculated pH for the ATom flight.
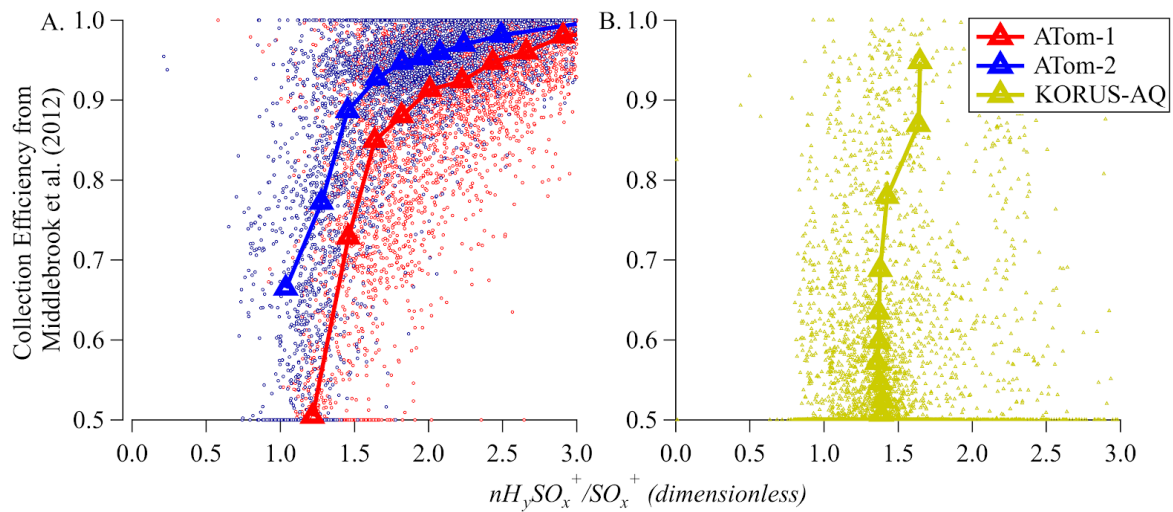
Fig. 8. (A) Collection efficiency parameterization vs. $nH_ySO_x^+/SO_x^+$ for two ATom campaigns, and (B) the KORUS-AQ campaign.

References

Ackendorf, J. M., Ippolito, M. G. and Galloway, M. M.: pH Dependence of the Imidazole-2-carboxaldehyde Hydration Equilibrium: Implications for Atmospheric Light Absorbance, Environ. Sci. Technol. Lett., 4(12), 551–555, doi:10.1021/acs.estlett.7b00486, 2017.

Alfarra, M. R., Coe, H., Allan, J. D., Bower, K. N., Boudries, H., Canagaratna, M. R., Jimenez, J. L., Jayne, J. T., Garforth, A. A., Li, S.-M. and Worsnop, D. R.: Characterization of urban and rural organic particulate in the Lower Fraser Valley using two Aerodyne Aerosol Mass Spectrometers, Atmos. Environ., 38(34), 5745–5758, doi:10.1016/j.atmosenv.2004.01.054, 2004.

Allan, J. D., Delia, A. E., Coe, H., Bower, K. N., Alfarra, M. R., Jimenez, J. L., Middlebrook, A. M., Drewnick, F., Onasch, T. B., Canagaratna, M. R., Jayne, J. T. and Worsnop, D. R.: A generalised method for the extraction of chemically resolved mass spectra from Aerodyne aerosol mass spectrometer data, J. Aerosol Sci., 35(7), 909–922, doi:10.1016/j.jaerosci.2004.02.007, 2004.

Anon: Atmospheric chemistry and physics: from air pollution to climate change, Choice Reviews Online, 44(08), 44–4512–44–4512, doi:10.5860/CHOICE.44-4512, 2007.

Bahreini, R., Dunlea, E. J., Matthew, B. M., Simons, C., Docherty, K. S., DeCarlo, P. F., Jimenez, J. L., Brock, C. A. and Middlebrook, A. M.: Design and Operation of a Pressure-Controlled Inlet for Airborne Sampling with an Aerodynamic Aerosol Lens, Aerosol Sci. Technol., 42(6), 465–471, doi:10.1080/02786820802178514, 2008.

Bahreini, R., Ervens, B., Middlebrook, A. M., Warneke, C., de Gouw, J. A., DeCarlo, P. F., Jimenez, J. L., Brock, C. A., Neuman, J. A., Ryerson, T. B., Stark, H., Atlas, E., Brioude, J., Fried, A., Holloway, J. S., Peischl, J., Richter, D., Walega, J., Weibring, P., Wollny, A. G. and Fehsenfeld, F. C.: Organic aerosol formation in urban and industrial plumes near Houston and Dallas, Texas, J. Geophys. Res., 114, 1185, doi:10.1029/2008JD011493, 2009.

Barth, M. C., Cantrell, C. A., Brune, W. H., Rutledge, S. A., Crawford, J. H., Huntrieser, H., Carey, L. D., MacGorman, D., Weisman, M., Pickering, K. E., Bruning, E., Anderson, B., Apel, E., Biggerstaff, M., Campos, T., Campuzano-Jost, P., Cohen, R., Crounse, J., Day, D. A., Diskin, G., Flocke, F., Fried, A., Garland, C., Heikes, B., Honomichl, S., Hornbrook, R., Huey, L. G., Jimenez, J. L., Lang, T., Lichtenstern, M., Mikoviny, T., Nault, B., O'Sullivan, D., Pan, L. L., Peischl, J., Pollack, I., Richter, D., Riemer, D., Ryerson, T., Schlager, H., St. Clair, J., Walega, J., Weibring, P., Weinheimer, A., Wennberg, P., Wisthaler, A., Wooldridge, P. J. and Ziegler, C.: The Deep Convective Clouds and Chemistry (DC3) Field Campaign, Bull. Am. Meteorol. Soc., 96(8), 1281–1309, doi:10.1175/BAMS-D-13-00290.1, 2015.

Bertram, T. H. and Thornton, J. A.: Toward a general parameterization of N_2O_5 reactivity on aqueous particles: the competing effects of particle liquid water, nitrate and chloride, Atmos.

854 Chem. Phys., 9(21), 8351–8363, 2009.

855 Bey, I., Jacob, D. J., Yantosca, R. M., Logan, J. A., Field, B. D., Fiore, A. M., Li, Q., Liu, H. Y.,
856 Mickley, L. J. and Schultz, M. G.: Global modeling of tropospheric chemistry with assimilated
857 meteorology: Model description and evaluation, J. Geophys. Res., 106(D19), 23073–23095,
858 doi:10.1029/2001JD000807, 2001.

859 Brock, C.: Aerosol size distributions during the Atmospheric Tomography (ATom) mission:
860 methods, uncertainties, and data products, Aerosols/In Situ Measurement/Instruments and
861 Platforms/amt-2019-44, doi:10.5194/amt-2019-44-ac1, 2019.

862 Brüggemann, M., Riva, M., Perrier, S., Poulain, L., George, C. and Herrmann, H.:
863 Overestimation of Monoterpene Organosulfate Abundance in Aerosol Particles by Sampling in
864 the Presence of SO2, Environ. Sci. Technol. Lett., doi:10.1021/acs.estlett.0c00814, 2020.

865 Canagaratna, M. R., Jayne, J. T., Jimenez, J. L., Allan, J. D., Alfarra, M. R., Zhang, Q., Onasch,
866 T. B., Drewnick, F., Coe, H., Middlebrook, A., Delia, A., Williams, L. R., Trimborn, A. M.,
867 Northway, M. J., DeCarlo, P. F., Kolb, C. E., Davidovits, P. and Worsnop, D. R.: Chemical and
868 microphysical characterization of ambient aerosols with the aerodyne aerosol mass spectrometer,
869 Mass Spectrom. Rev., 26(2), 185–222, doi:10.1002/mas.20115, 2007.

870 Carlton, A. G., de Gouw, J., Jimenez, J. L., Ambrose, J. L., Attwood, A. R., Brown, S., Baker, K.
871 R., Brock, C., Cohen, R. C., Edgerton, S., Farkas, C. M., Farmer, D., Goldstein, A. H., Gratz, L.,
872 Guenther, A., Hunt, S., Jaeglé, L., Jaffe, D. A., Mak, J., McClure, C., Nenes, A., Nguyen, T. K.,
873 Pierce, J. R., de Sa, S., Selin, N. E., Shah, V., Shaw, S., Shepson, P. B., Song, S., Stutz, J.,
874 Surratt, J. D., Turpin, B. J., Warneke, C., Washenfelder, R. A., Wennberg, P. O. and Zhou, X.:
875 Synthesis of the Southeast Atmosphere Studies: Investigating Fundamental Atmospheric
876 Chemistry Questions, Bull. Am. Meteorol. Soc., 99(3), 547–567,
877 doi:10.1175/BAMS-D-16-0048.1, 2018.

878 Chen, Y., Xu, L., Humphry, T., Hettiyadura, A. P. S., Ovadnevaite, J., Huang, S., Poulain, L.,
879 Schroder, J. C., Campuzano-Jost, P., Jimenez, J. L., Herrmann, H., O'Dowd, C., Stone, E. A. and
880 Ng, N. L.: Response of the Aerodyne Aerosol Mass Spectrometer to Inorganic Sulfates and
881 Organosulfur Compounds: Applications in Field and Laboratory Measurements, Environ. Sci.
882 Technol., 53(9), 5176–5186, doi:10.1021/acs.est.9b00884, 2019.

883 Clegg, S. L., Brimblecombe, P. and Wexler, A. S.: Thermodynamic Model of the System H +
884 -NH 4 + -SO 42- -NO 3 - -H 2 O at Tropospheric Temperatures, , 5639(3), 2137–2154, 1998a.

885 Clegg, S. L., Brimblecombe, P. and Wexler, A. S.: Thermodynamic Model of the System H
886 −NH4 −SO42-−NO3-−H2O at Tropospheric Temperatures, The Journal of Physical Chemistry
887 A, 102(12), 2137–2154, doi:10.1021/jp973042r, 1998b.

888 Clegg, S. L., Seinfeld, J. H. and Edney, E. O.: Thermodynamic modelling of aqueous aerosols
889 containing electrolytes and dissolved organic compounds. II. An extended
890 Zdanovskii–Stokes–Robinson approach, J. Aerosol Sci., 34(6), 667–690,

891 doi:10.1016/S0021-8502(03)00019-3, 2003.

892 Craig, R. L., Peterson, P. K., Nandy, L., Lei, Z., Hossain, M. A., Camarena, S., Dodson, R. A.,
893 Cook, R. D., Dutcher, C. S. and Ault, A. P.: Direct Determination of Aerosol pH: Size-Resolved
894 Measurements of Submicrometer and Supermicrometer Aqueous Particles, Anal. Chem., 90(19),
895 11232–11239, doi:10.1021/acs.analchem.8b00586, 2018.

896 Crounse, J. D., McKinney, K. A., Kwan, A. J. and Wennberg, P. O.: Measurement of gas-phase
897 hydroperoxides by chemical ionization mass spectrometry, Anal. Chem., 78(19), 6726–6732,
898 doi:10.1021/ac0604235, 2006.

899 Cubison, M. J., Ortega, A. M., Hayes, P. L., Farmer, D. K., Day, D., Lechner, M. J., Brune, W.
900 H., Apel, E., Diskin, G. S., Fisher, J. A. and Others: Effects of aging on organic aerosol from
901 open biomass burning smoke in aircraft and laboratory studies, Atmos. Chem. Phys., 11(23),
902 12049–12064 [online] Available from:
903 https://www.atmos-chem-phys.net/11/12049/2011/acp-11-12049-2011.pdf, 2011.

904 DeCarlo, P. F., Kimmel, J. R., Trimborn, A., Northway, M. J., Jayne, J. T., Aiken, A. C., Gonin,
905 M., Fuhrer, K., Horvath, T., Docherty, K. S., Worsnop, D. R. and Jimenez, J. L.:
906 Field-deployable, high-resolution, time-of-flight aerosol mass spectrometer, Anal. Chem.,
907 78(24), 8281–8289, doi:10.1021/ac061249n, 2006.

908 DeCarlo, P. F., Dunlea, E. J., Kimmel, J. R., Aiken, A. C., Sueper, D., Crounse, J., Wennberg, P.
909 O., Emmons, L., Shinozuka, Y., Clarke, A. and Others: Fast airborne aerosol size and chemistry
910 measurements above Mexico City and Central Mexico during the MILAGRO campaign, 1foldr
911 Import 2019-10-08 Batch 1 [online] Available from:
912 https://oaktrust.library.tamu.edu/bitstream/handle/1969.1/178622/document-2.pdf?sequence=2,
913 2008.

914 Dentener, F. J. and Crutzen, P. J.: A three-dimensional model of the global ammonia cycle, J.
915 Atmos. Chem., 19(4), 331–369, doi:10.1007/BF00694492, 1994.

916 Docherty, K. S., Lewandowski, M. and Jimenez, J. L.: Effect of Vaporizer Temperature on
917 Ambient Non-Refractory Submicron Aerosol Composition and Mass Spectra Measured by the
918 Aerosol Mass Spectrometer, Aerosol Sci. Technol., 49(7), 485–494,
919 doi:10.1080/02786826.2015.1042100, 2015.

920 Dockery, D. W., Cunningham, J., Damokosh, A. I., Neas, L. M., Spengler, J. D., Koutrakis, P.,
921 Ware, J. H., Raizenne, M. and Speizer, F. E.: Health effects of acid aerosols on North American
922 children: respiratory symptoms, Environ. Health Perspect., 104(5), 500–505,
923 doi:10.1289/ehp.96104500, 1996.

924 Dovrou, E., Lim, C. Y., Canagaratna, M. R., Kroll, J. H., Worsnop, D. R. and Keutsch, F. N.:
925 Measurement techniques for identifying and quantifying hydroxymethanesulfonate (HMS) in an
926 aqueous matrix and particulate matter using aerosol mass spectrometry and ion chromatography,
927 Atmospheric Measurement Techniques, 12(10), 5303–5315, doi:10.5194/amt-12-5303-2019,

2019.

Dunlea, E. J., DeCarlo, P. F., Aiken, A. C., Kimmel, J. R., Peltier, R. E., Weber, R. J., Tomlinson, J., Collins, D. R., Shinozuka, Y., McNaughton, C. S. and Others: Evolution of Asian aerosols during transpacific transport in INTEX-B, Atmos. Chem. Phys., 9(19), 7257–7287 [online] Available from: https://www.atmos-chem-phys.net/9/7257/2009/acp-9-7257-2009.pdf, 2009.

Facchini, M. C., Decesari, S., Rinaldi, M., Carbone, C., Finessi, E., Mircea, M., Fuzzi, S., Moretti, F., Tagliavini, E., Ceburnis, D. and O'Dowd, C. D.: Important source of marine secondary organic aerosol from biogenic amines, Environ. Sci. Technol., 42(24), 9116–9121, doi:10.1021/es8018385, 2008.

Farmer, D. K., Matsunaga, A., Docherty, K. S., Surratt, J. D., Seinfeld, J. H., Ziemann, P. J. and Jimenez, J. L.: Response of an aerosol mass spectrometer to organonitrates and organosulfates and implications for atmospheric chemistry, Proc. Natl. Acad. Sci. U. S. A., 107(15), 6670–6675, doi:10.1073/pnas.0912340107, 2010.

Fountoukis, C. and Nenes, A.: ISORROPIA II: a computationally efficient thermodynamic equilibrium model for K^+–Ca^{2+}–Mg^{2+}–NH_4^+–Na^+–SO_4^{2-}–NO_3^-–Cl^-–H_2O aero, Atmos. Chem. Phys., 7(17), 4639–4659, doi:10.5194/acp-7-4639-2007, 2007.

Friese, E. and Ebel, A.: Temperature Dependent Thermodynamic Model of the System H −NH4 −Na −SO42−−NO3−−Cl−−H2O, The Journal of Physical Chemistry A, 114(43), 11595–11631, doi:10.1021/jp101041j, 2010.

Frossard, A. a., Russell, L. M., Burrows, S. M., Elliott, S. M., Bates, T. S. and Quinn, P. K.: Sources and Composition of Submicron Organic Mass in Marine Aerosol Particles, J. Geophys. Res. D: Atmos., doi:10.1002/2014JD021913, 2014.

Froyd, K. D., Murphy, D. M., Sanford, T. J., Thomson, D. S., Wilson, J. C., Pfister, L. and Lait, L.: Aerosol composition of the tropical upper troposphere, Atmos. Chem. Phys., 9(13), 4363–4385, doi:10.5194/acp-9-4363-2009, 2009.

Froyd, K. D., Murphy, D. M., Brock, C. A., Campuzano-Jost, P., Dibb, J. E., Jimenez, J.-L., Kupc, A., Middlebrook, A. M., Schill, G. P., Thornhill, K. L., Williamson, C. J., Wilson, J. C. and Ziemba, L. D.: A new method to quantify mineral dust and other aerosol species from aircraft platforms using single-particle mass spectrometry, Atmospheric Measurement Techniques, 12(11), 6209–6239, doi:10.5194/amt-12-6209-2019, 2019.

Fry, J. L., Draper, D. C., Zarzana, K. J., Campuzano-Jost, P., Day, D. A., Jimenez, J. L., Brown, S. S., Cohen, R. C., Kaser, L., Hansel, A., Cappellin, L., Karl, T., Hodzic Roux, A., Turnipseed, A., Cantrell, C., Lefer, B. L. and Grossberg, N.: Observations of gas- and aerosol-phase organic nitrates at BEACHON-RoMBAS 2011, Atmospheric Chemistry and Physics, 13(17), 8585–8605, doi:10.5194/acp-13-8585-2013, 2013.

Gaston, C. J., Riedel, T. P., Zhang, Z., Gold, A., Surratt, J. D. and Thornton, J. A.: Reactive Uptake of an Isoprene-Derived Epoxydiol to Submicron Aerosol Particles, ,

965 doi:10.1021/es5034266, 2014.

966 Gelaro, R., McCarty, W., Suárez, M. J., Todling, R., Molod, A., Takacs, L., Randles, C. A.,
967 Darmenov, A., Bosilovich, M. G., Reichle, R., Wargan, K., Coy, L., Cullather, R., Draper, C.,
968 Akella, S., Buchard, V., Conaty, A., da Silva, A. M., Gu, W., Kim, G.-K., Koster, R., Lucchesi,
969 R., Merkova, D., Nielsen, J. E., Partyka, G., Pawson, S., Putman, W., Rienecker, M., Schubert, S.
970 D., Sienkiewicz, M. and Zhao, B.: The Modern-Era Retrospective Analysis for Research and
971 Applications, Version 2 (MERRA-2), J. Clim., 30(14), 5419–5454,
972 doi:10.1175/JCLI-D-16-0758.1, 2017.

973 Ge, X., Shaw, S. L. and Zhang, Q.: Toward Understanding Amines and Their Degradation
974 Products from Postcombustion CO2 Capture Processes with Aerosol Mass Spectrometry,
975 Environ. Sci. Technol. [online] Available from: http://pubs.acs.org/doi/abs/10.1021/es4056966,
976 2014.

977 Gibb, S. W., Mantoura, R. F. C. and Liss, P. S.: Ocean-atmosphere exchange and atmospheric
978 speciation of ammonia and methylamines in the region of the NW Arabian Sea, Global
979 Biogeochemical Cycles, 13(1), 161–178, doi:10.1029/98gb00743, 1999.

980 Giglio, L., Randerson, J. T. and van der Werf, G. R.: Analysis of daily, monthly, and annual
981 burned area using the fourth-generation global fire emissions database (GFED4), Journal of
982 Geophysical Research: Biogeosciences, 118(1), 317–328 [online] Available from:
983 https://agupubs.onlinelibrary.wiley.com/doi/abs/10.1002/jgrg.20042, 2013.

984 Guo, H., Xu, L., Bougiatioti, A., Cerully, K. M., Capps, S. L., Hite, J. R., Jr, Carlton, A. G., Lee,
985 S.-H., Bergin, M. H., Ng, N. L. and Others: Fine-particle water and pH in the southeastern
986 United States, Atmospheric Chemistry & Physics, 15(9) [online] Available from:
987 https://www.researchgate.net/profile/Kate_Cerully/publication/276206260_Fine-particle_water_
988 and_pH_in_the_southeastern_United_States/links/55f6fc8508aeba1d9eee4213.pdf, 2015.

989 Guo, H., Sullivan, A. P., Campuzano-Jost, P., Schroder, J. C., Lopez-Hilfiker, F. D., Dibb, J. E.,
990 Jimenez, J. L., Thornton, J. A., Brown, S. S., Nenes, A. and Others: Fine particle pH and the
991 partitioning of nitric acid during winter in the northeastern United States, J. Geophys. Res. D:
992 Atmos., 121(17), 10–355 [online] Available from:
993 https://onlinelibrary.wiley.com/doi/pdf/10.1002/2016JD025311, 2016.

994 Guo, H., Liu, J., Froyd, K. D., Roberts, J. M., Veres, P. R., Hayes, P. L., Jimenez, J. L., Nenes, A.
995 and Weber, R. J.: Fine particle pH and gas–particle phase partitioning of inorganic species in
996 Pasadena, California, during the 2010 CalNex campaign, Atmospheric Chemistry and Physics,
997 17(9), 5703–5719, doi:10.5194/acp-17-5703-2017, 2017.

998 Guo, H., Campuzano-Jost, P., Nault, B. A., Day, D. A., Schroder, J. C., Dibb, J. E., Dollner, M.,
999 Weinzierl, B. and Jimenez, J. L.: The Importance of Size Ranges in Aerosol Instrument
1000 Intercomparisons: A Case Study for the ATom Mission, , doi:10.5194/amt-2020-224, 2020.

1001 Hennigan, C. J., Sullivan, A. P., Fountoukis, C. I., Nenes, A., Hecobian, A., Vargas, O., Hanks,

A. T. C., Huey, L. G., Lefer, B. L., Russell, A. G. and Others: On the volatility and production mechanisms of newly formed nitrate and water soluble organic aerosol in Mexico City, [online] Available from: https://hal.archives-ouvertes.fr/hal-00304021/, 2008.

Hennigan, C. J., Izumi, J., Sullivan, A. P., Weber, R. J. and Nenes, A.: A critical evaluation of proxy methods used to estimate the acidity of atmospheric particles, Atmos. Chem. Phys., 15(5), 2775 [online] Available from: https://pdfs.semanticscholar.org/18b0/f81231da34dbf1e29d753ae7c5e111cbd7fb.pdf, 2015.

Hodshire, A. L., Campuzano-Jost, P., Kodros, J. K., Croft, B., Nault, B. A., Schroder, J. C., Jimenez, J. L. and Pierce, J. R.: The potential role of methanesulfonic acid (MSA) in aerosol formation and growth and the associated radiative forcings, Atmos. Chem. Phys., 19(5), 3137–3160, doi:10.5194/acp-19-3137-2019, 2019.

Hodzic, A., Campuzano-Jost, P., Bian, H., Chin, M., Colarco, P. R., Day, D. A., Froyd, K. D., Heinold, B., Jo, D. S., Katich, J. M. and Others: Characterization of Organic Aerosol across the Global Remote Troposphere: A comparison of ATom measurements and global chemistry models, Atmos. Chem. Phys., 2020.

Hoesly, R. M., Smith, S. J., Feng, L., Klimont, Z., Janssens-Maenhout, G., Pitkanen, T., Seibert, J. J., Vu, L., Andres, R. J., Bolt, R. M. and Others: Historical (1750--2014) anthropogenic emissions of reactive gases and aerosols from the Community Emissions Data System (CEDS), Geoscientific Model Development (Online), 11(PNNL-SA-123932) [online] Available from: https://www.osti.gov/biblio/1421326, 2018.

Huang, S., Poulain, L., van Pinxteren, D., van Pinxteren, M., Wu, Z., Herrmann, H. and Wiedensohler, A.: Latitudinal and Seasonal Distribution of Particulate MSA over the Atlantic using a Validated Quantification Method with HR-ToF-AMS, Environ. Sci. Technol., 51(1), 418–426, doi:10.1021/acs.est.6b03186, 2017.

Huffman, J. A., Jayne, J. T., Drewnick, F., Aiken, A. C., Onasch, T., Worsnop, D. R. and Jimenez, J. L.: Design, Modeling, Optimization, and Experimental Tests of a Particle Beam Width Probe for the Aerodyne Aerosol Mass Spectrometer, Aerosol Sci. Technol., 39(12), 1143–1163, doi:10.1080/02786820500423782, 2005.

Hu, W., Campuzano-Jost, P., Day, D. A., Croteau, P., Canagaratna, M. R., Jayne, J. T., Worsnop, D. R. and Jimenez, J. L.: Evaluation of the new capture vaporizer for aerosol mass spectrometers (AMS) through field studies of inorganic species, Aerosol Sci. Technol., 51(6), 735–754, doi:10.1080/02786826.2017.1296104, 2017a.

Hu, W., Campuzano-Jost, P., Day, D. A., Croteau, P., Canagaratna, M. R., Jayne, J. T., Worsnop, D. R. and Jimenez, J. L.: Evaluation of the new capture vapourizer for aerosol mass spectrometers (AMS) through laboratory studies of inorganic species, Atmospheric Measurement Techniques, 10(8), doi:10.5194/amt-10-2897-2017, 2017b.

Hu, W., Campuzano-Jost, P., Day, D. A., Nault, B., Park, T., Lee, T., Pajunoja, A., Virtanen, A.,

Croteau, P. L., Canagaratna, M. R., Jayne, J. T., Worsnop, D. R. and Jimenez, J. L.: Ambient quantification and size distributions for organic aerosol (OA) in aerosol mass spectrometer (AMS) instruments with the new capture vaporizer (CV), ACS Earth and Space Chemistry, doi:10.1021/acsearthspacechem.9b00310, 2020.

Hu, W. W., Campuzano-Jost, P., Palm, B. B., Day, D. A., Ortega, A. M., Hayes, P. L., Krechmer, J. E., Chen, Q., Kuwata, M., Liu, Y. J. and Others: Characterization of a real-time tracer for isoprene epoxydiols-derived secondary organic aerosol (IEPOX-SOA) from aerosol mass spectrometer measurements, Atmos. Chem. Phys., 15(20), 11807–11833 [online] Available from: https://www.atmos-chem-phys.net/15/11807/2015/acp-15-11807-2015.html, 2015.

IPCC: IPCC 2013: Climate Change 2013: The Physical Science Basis. Contribution of Working Group I to the Fifth Assessment Report of the Intergovernmental Panel on Climate Change, edited by T. F. Stocker, D. Qin, G. K. Plattner, M. Tignor, S. K. Allen, V. Bex, and P. M. Midgley, Cambridge University Press, Cambridge, United Kingdom and New York, NY, USA., 2013.

Jaeglé, L., Shah, V., Thornton, J. A., Lopez-Hilfiker, F. D., Lee, B. H., McDuffie, E. E., Fibiger, D., Brown, S. S., Veres, P., Sparks, T., Ebben, C., Wooldridge, P. J., Kenagy, H. S., Cohen, R. C., Weinheimer, A. J., Campos, T. L., Montzka, D. D., Digangi, J. P., Wolfe, G. M., Hanisco, T., Schroder, J. C., Campuzano-Jost, P., Day, D. A., Jimenez, J. L., Sullivan, A. P., Guo, H. and Weber, R. J.: Nitrogen Oxides Emissions , Chemistry , Deposition , and Export Over the Northeast United States During the WINTER Aircraft Campaign, J. Geophys. Res. D: Atmos., (2), 368–393, doi:10.1029/2018JD029133, 2018.

Jang, M., Czoschke, N. M., Lee, S. and Kamens, R. M.: Heterogeneous atmospheric aerosol production by acid-catalyzed particle-phase reactions, Science, 298(5594), 814–817, doi:10.1126/science.1075798, 2002.

Jayne, J. T., Leard, D. C., Zhang, X., Davidovits, P., Smith, K. A., Kolb, C. E. and Worsnop, D. R.: Development of an Aerosol Mass Spectrometer for Size and Composition Analysis of Submicron Particles, Aerosol Sci. Technol., 33(1-2), 49–70, doi:10.1080/027868200410840, 2000.

Jimenez, J. L., Jayne, J. T., Shi, Q., Kolb, C. E., Worsnop, D. R., Yourshaw, I., Seinfeld, J. H., Flagan, R. C., Zhang, X. F., Smith, K. A., Morris, J. W. and Davidovits, P.: Ambient aerosol sampling using the Aerodyne Aerosol Mass Spectrometer, J. Geophys. Res., 108(D7), 8425–8425, doi:10.1029/2001JD001213, 2003.

Jimenez, J. L., Canagaratna, M. R., Donahue, N. M., Prevot, A. S. H., Zhang, Q., Kroll, J. H., DeCarlo, P. F., Allan, J. D., Coe, H., Ng, N. L., Aiken, A. C., Docherty, K. S., Ulbrich, I. M., Grieshop, A. P., Robinson, A. L., Duplissy, J., Smith, J. D., Wilson, K. R., Lanz, V. A., Hueglin, C., Sun, Y. L., Tian, J., Laaksonen, A., Raatikainen, T., Rautiainen, J., Vaattovaara, P., Ehn, M., Kulmala, M., Tomlinson, J. M., Collins, D. R., Cubison, M. J., Dunlea, E. J., Huffman, J. A., Onasch, T. B., Alfarra, M. R., Williams, P. I., Bower, K., Kondo, Y., Schneider, J., Drewnick, F., Borrmann, S., Weimer, S., Demerjian, K., Salcedo, D., Cottrell, L., Griffin, R., Takami, A.,

Miyoshi, T., Hatakeyama, S., Shimono, A., Sun, J. Y., Zhang, Y. M., Dzepina, K., Kimmel, J. R., Sueper, D., Jayne, J. T., Herndon, S. C., Trimborn, A. M., Williams, L. R., Wood, E. C., Middlebrook, A. M., Kolb, C. E., Baltensperger, U. and Worsnop, D. R.: Evolution of organic aerosols in the atmosphere, Science, 326(5959), 1525–1529, doi:10.1126/science.1180353, 2009.

Jo, D. S., Hodzic, A., Emmons, L. K., Marais, E. A., Peng, Z., Nault, B. A., Hu, W., Campuzano-Jost, P. and Jimenez, J. L.: A simplified parameterization of isoprene-epoxydiol-derived secondary organic aerosol (IEPOX-SOA) for global chemistry and climate models: a case study with GEOS-Chem v11-02-rc, Geoscientific Model Development, 12(7), 2983–3000, doi:10.5194/gmd-12-2983-2019, 2019.

Johnson, K. S., Laskin, A., Jimenez, J. L., Shutthanandan, V., Molina, L. T., Salcedo, D., Dzepina, K. and Molina, M. J.: Comparative analysis of urban atmospheric aerosol by particle-induced X-ray emission (PIXE), proton elastic scattering analysis (PESA), and aerosol mass spectrometry (AMS), Environ. Sci. Technol., 42(17), 6619–6624, doi:10.1021/es800393e, 2008.

Kang, H., Day, D. A., Krechmer, J. E., Ayres, B. R., Keehan, N. I., Thompson, S. L., Hu, W., Campuzano-Jost, P., Schroder, J. C., Stark, H., Ranney, A., Ziemann, P., Zarzana, K. J., Wild, R. J., Dubé, W., Brown, S. S., Fry, J. and Jimenez, J. L.: A33E-0280: Secondary organic aerosol mass yields from the dark NO3 oxidation of α-pinene and-carene: effect of RO2 radical fate, in American Geophysical Union Fall Meeting., San Francisco, CA, USA, 12-16 December 2016.

Keene, W. C.: Variation of marine aerosol acidity with particle size, Geophys. Res. Lett., 29(7), 20,565, doi:10.1029/2001GL013881, 2002.

Lambert, J. B.: Organic structural spectroscopy, Pearson College Division., 1998.

Lee, B. H., Lopez-Hilfiker, F. D., Mohr, C., Kurtén, T., Worsnop, D. R. and Thornton, J. a.: An iodide-adduct high-resolution time-of-flight chemical-ionization mass spectrometer: application to atmospheric inorganic and organic compounds, Environ. Sci. Technol., 48(11), 6309–6317, doi:10.1021/es500362a, 2014.

Lee, B. H., Lopez-Hilfiker, F. D., Veres, P. R., McDuffie, E. E., Fibiger, D. L., Sparks, T. L., Ebben, C. J., Green, J. R., Schroder, J. C., Campuzano-Jost, P. and Others: Flight deployment of a high-resolution time-of-flight chemical ionization mass spectrometer: Observations of reactive halogen and nitrogen oxide species, J. Geophys. Res. D: Atmos., 123(14), 7670–7686 [online] Available from: https://agupubs.onlinelibrary.wiley.com/doi/abs/10.1029/2017JD028082@10.1002/(ISSN)2169-8996.WINTER1, 2018.

Lee, T., Sullivan, A. P., Mack, L., Jimenez, J. L., Kreidenweis, S. M., Onasch, T. B., Worsnop, D. R., Malm, W., Wold, C. E., Hao, W. M. and Collett, J. L.: Chemical Smoke Marker Emissions During Flaming and Smoldering Phases of Laboratory Open Burning of Wildland Fuels, Aerosol Sci. Technol., 44(9), i–v, doi:10.1080/02786826.2010.499884, 2010.

Liao, J., Froyd, K. D., Murphy, D. M., Keutsch, F. N., Yu, G., Wennberg, P. O., Clair, J. M. S., Crounse, J. D., Wisthaler, A., Mikoviny, T. and Others: Airborne measurements of organosulfates over the continental US, J. Geophys. Res. D: Atmos., 120(7), 2990–3005 [online] Available from: https://agupubs.onlinelibrary.wiley.com/doi/abs/10.1002/2014JD022378%4010.1002/%28ISSN %292169-8996.SEAFOURC1, 2015.

Li, G., Bei, N., Cao, J., Huang, R., Wu, J., Feng, T., Wang, Y., Liu, S., Zhang, Q., Tie, X. and Molina, L. T.: A possible pathway for rapid growth of sulfate during haze days in China, , 3301–3316 [online] Available from: https://dspace.mit.edu/handle/1721.1/109728?show=full (Accessed 2 August 2019), 2017.

Lighty, J. S., Veranth, J. M. and Sarofim, A. F.: Combustion aerosols: factors governing their size and composition and implications to human health, J. Air Waste Manag. Assoc., 50(9), 1565–618; discussion 1619–22 [online] Available from: https://www.ncbi.nlm.nih.gov/pubmed/11055157, 2000.

Liu, P., Ziemann, P. J., Kittelson, D. B. and McMurry, P. H.: Generating Particle Beams of Controlled Dimensions and Divergence: II. Experimental Evaluation of Particle Motion in Aerodynamic Lenses and Nozzle Expansions, Aerosol Sci. Technol., 22(3), 314–324, doi:10.1080/02786829408959749, 1995.

Liu, X., Day, D. A., Krechmer, J. E., Brown, W., Peng, Z., Ziemann, P. J. and Jimenez, J. L.: Direct measurements of semi-volatile organic compound dynamics show near-unity mass accommodation coefficients for diverse aerosols, Communications Chemistry, 2(1), 1–9, doi:10.1038/s42004-019-0200-x, 2019.

Lohmann, U., Broekhuizen, K., Leaitch, R., Shantz, N. and Abbatt, J.: How efficient is cloud droplet formation of organic aerosols?, Geophys. Res. Lett., 31(5), 2004.

Losey, D. J., Ott, E.-J. E. and Freedman, M. A.: Effects of High Acidity on Phase Transitions of an Organic Aerosol, J. Phys. Chem. A, 122(15), 3819–3828, doi:10.1021/acs.jpca.8b00399, 2018.

Massucci, M., Clegg, S. L. and Brimblecombe, P.: Equilibrium Partial Pressures, Thermodynamic Properties of Aqueous and Solid Phases, and Cl2 Production from Aqueous HCl and HNO3 and Their Mixtures, J. Phys. Chem. A, 103(21), 4209–4226, doi:10.1021/jp9847179, 1999.

Matthew, B. M., Middlebrook, A. M. and Onasch, T. B.: Collection Efficiencies in an Aerodyne Aerosol Mass Spectrometer as a Function of Particle Phase for Laboratory Generated Aerosols, Aerosol Sci. Technol., 42(11), 884–898, doi:10.1080/02786820802356797, 2008.

Meskhidze, N., Chameides, W. L., Nenes, A. and Chen, G.: Iron mobilization in mineral dust: Can anthropogenic SO2 emissions affect ocean productivity?, Geophys. Res. Lett., 30(21) [online] Available from:

1152 https://agupubs.onlinelibrary.wiley.com/doi/abs/10.1029/2003GL018035, 2003.

1153 Middlebrook, A. M., Bahreini, R., Jimenez, J. L. and Canagaratna, M. R.: Evaluation of
1154 Composition-Dependent Collection Efficiencies for the Aerodyne Aerosol Mass Spectrometer
1155 using Field Data, Aerosol Sci. Technol., 46(3), 258–271, doi:10.1080/02786826.2011.620041,
1156 2012.

1157 Müller, C., Iinuma, Y., Karstensen, J., Van Pinxteren, D., Lehmann, S., Gnauk, T. and Herrmann,
1158 H.: Seasonal variation of aliphatic amines in marine sub-micrometer particles at the Cape Verde
1159 islands, [online] Available from: https://oar.tib.eu/jspui/handle/123456789/261, 2009.

1160 Murphy, S. M., Sorooshian, A., Kroll, J. H., Ng, N. L., Chhabra, P., Tong, C., Surratt, J. D.,
1161 Knipping, E., Flagan, R. C. and Seinfeld, J. H.: Secondary aerosol formation from atmospheric
1162 reactions of aliphatic amines, Atmospheric Chemistry and Physics Discussions, 7(1), 289–349,
1163 doi:10.5194/acpd-7-289-2007, 2007.

1164 Nault, B. A., Campuzano-Jost, P., Day, D. A., Schroder, J. C., Anderson, B., Beyersdorf, A. J.,
1165 Blake, D. R., Brune, W. H., Choi, Y., Corr, C. A., Gouw, J. A. de, Dibb, J., DiGangi, J. P., Diskin,
1166 G. S., Fried, A., Huey, L. G., Kim, M. J., Knote, C. J., Lamb, K. D., Lee, T., Park, T., Pusede, S.
1167 E., Scheuer, E., Thornhill, K. L., Woo, J.-H. and Jimenez, J. L.: Secondary organic aerosol
1168 production from local emissions dominates the organic aerosol budget over Seoul, South Korea,
1169 during KORUS-AQ, Atmos. Chem. Phys., 18(24), 17769–17800,
1170 doi:10.5194/acp-18-17769-2018, 2018.

1171 Nault, B. A., Campuzano-Jost, P., Jo, D., Day, D., Bahreini, R., Bian, H., Chin, M., Clegg, S.,
1172 Colarco, P., Kodros, J., Lopez-Hilfiker, F., Marais, E., Middlebrook, A., Neuman, A., Nowak, J.,
1173 Pierce, J., Thornton, J., Tsigaridis, K., Jimenez, J. and ATom Science Team: Global Survey of
1174 Aerosol Acidity from Polluted to Remote Locations: Measurements and Comparisons with
1175 Global Models, display, doi:10.5194/egusphere-egu2020-11366, 2020.

1176 Nault, B. A., Campuzano-Jost, P., Day, D. A., Jo, D. S., Schroder, J. S., Allen, H. M., Bahreini,
1177 R., Bian, H., Blake, D. R., Chin, M., Clegg, S. L., Colarco, P. R., Crounse, J. D., Cubison, M. J.,
1178 DeCarlo, P. F., Dibb, J. E., Diskin, G. S., Hodzic, A., Hu, W., Katich, J., Kim, M. J., Kodros, J.
1179 K., Kupc, A., Lopez-Hilfiker, F. D., Marais, E. A., Middlebrook, A. M., Neuman, J. A., Nowak,
1180 J. B., Palm, B. B., Paulot, F., Pierce, J. R., Schill, G. P., Scheuer, E., Thornton, J. A., Tsigaridis,
1181 K., Wennberg, P. O., Williamson, C. J. and Jimenez, J. L.: Models underestimate the increase of
1182 acidity with remoteness biasing radiative impact calculations, Communications Earth &
1183 Environment [submitted], 2021.

1184 Nenes, A., Pandis, S. N. and Pilinis, C.: Continued development and testing of a new
1185 thermodynamic aerosol module for urban and regional air quality models, Atmos. Environ.,
1186 33(10), 1553–1560, doi:10.1016/S1352-2310(98)00352-5, 1999.

1187 Ng, N. L., Herndon, S. C., Trimborn, A., Canagaratna, M. R., Croteau, P. L., Onasch, T. B.,
1188 Sueper, D., Worsnop, D. R., Zhang, Q., Sun, Y. L. and Jayne, J. T.: An Aerosol Chemical
1189 Speciation Monitor (ACSM) for Routine Monitoring of the Composition and Mass

Concentrations of Ambient Aerosol, Aerosol Sci. Technol., 45(7), 780–794, doi:10.1080/02786826.2011.560211, 2011a.

Ng, N. L., Canagaratna, M. R., Jimenez, J. L., Chhabra, P. S., Seinfeld, J. H. and Worsnop, D. R.: Changes in organic aerosol composition with aging inferred from aerosol mass spectra, Atmos. Chem. Phys., 11(13), 6465 [online] Available from: http://citeseerx.ist.psu.edu/viewdoc/download?doi=10.1.1.388.4858&rep=rep1&type=pdf, 2011b.

Ovadnevaite, J., Ceburnis, D., Canagaratna, M., Berresheim, H., Bialek, J., Martucci, G., Worsnop, D. R. and O'Dowd, C.: On the effect of wind speed on submicron sea salt mass concentrations and source fluxes, J. Geophys. Res. D: Atmos., 117(D16) [online] Available from: https://agupubs.onlinelibrary.wiley.com/doi/abs/10.1029/2011JD017379, 2012.

Paulot, F., Jacob, D. J., Johnson, M. T., Bell, T. G., Baker, A. R., Keene, W. C., Lima, I. D., Doney, S. C. and Stock, C. A.: Global oceanic emission of ammonia: Constraints from seawater and atmospheric observations, Global Biogeochem. Cycles, 29(8), 1165–1178, doi:10.1002/2015GB005106, 2015.

Phinney, L., Richard Leaitch, W., Lohmann, U., Boudries, H., Worsnop, D. R., Jayne, J. T., Toom-Sauntry, D., Wadleigh, M., Sharma, S. and Shantz, N.: Characterization of the aerosol over the sub-arctic north east Pacific Ocean, Deep Sea Res. Part 2 Top. Stud. Oceanogr., 53(20), 2410–2433, doi:10.1016/j.dsr2.2006.05.044, 2006.

van Pinxteren, M., Fiedler, B., van Pinxteren, D., Iinuma, Y., Körtzinger, A. and Herrmann, H.: Chemical characterization of sub-micrometer aerosol particles in the tropical Atlantic Ocean: marine and biomass burning influences, J. Atmos. Chem., 72(2), 105–125, doi:10.1007/s10874-015-9307-3, 2015.

Pye, H. O. T., Liao, H., Wu, S., Mickley, L. J., Jacob, D. J., Henze, D. K. and Seinfeld, J. H.: Effect of changes in climate and emissions on future sulfate-nitrate-ammonium aerosol levels in the United States, J. Geophys. Res. D: Atmos., 114(D1) [online] Available from: https://agupubs.onlinelibrary.wiley.com/doi/abs/10.1029/2008JD010701, 2009.

Pye, H. O. T., Nenes, A., Alexander, B., Ault, A. P., Barth, M. C., Clegg, S. L., Collett, J. L., Jr, Fahey, K. M., Hennigan, C. J., Herrmann, H. and Others: The Acidity of Atmospheric Particles and Clouds, UMBC Faculty Collection [online] Available from: https://www.atmos-chem-phys-discuss.net/acp-2019-889/acp-2019-889.pdf, 2019.

Quinn, P. K., Charlson, R. J. and Bates, T. S.: Simultaneous observations of ammonia in the atmosphere and ocean, Nature, 335(6188), 336–338, doi:10.1038/335336a0, 1988.

Quinn, P. K., Bates, T. S., Coffman, D., Onasch, T. B., Worsnop, D., Baynard, T., De Gouw, J. A., Goldan, P. D., Kuster, W. C., Williams, E. and Others: Impacts of sources and aging on submicrometer aerosol properties in the marine boundary layer across the Gulf of Maine, J. Geophys. Res. D: Atmos., 111(D23) [online] Available from:

1227 https://agupubs.onlinelibrary.wiley.com/doi/abs/10.1029/2006JD007582, 2006.

1228 Raizenne, M., Neas, L. M., Damokosh, A. I., Dockery, D. W., Spengler, J. D., Koutrakis, P.,
1229 Ware, J. H. and Speizer, F. E.: Health effects of acid aerosols on North American children:
1230 pulmonary function, Environ. Health Perspect., 104(5), 506–514, doi:10.1289/ehp.96104506,
1231 1996.

1232 Rindelaub, J. D., Craig, R. L., Nandy, L., Bondy, A. L., Dutcher, C. S., Shepson, P. B. and Ault,
1233 A. P.: Direct Measurement of pH in Individual Particles via Raman Microspectroscopy and
1234 Variation in Acidity with Relative Humidity, J. Phys. Chem. A, 120(6), 911–917,
1235 doi:10.1021/acs.jpca.5b12699, 2016.

1236 Riva, M., Budisulistiorini, S. H., Chen, Y., Zhang, Z., D'Ambro, E. L., Zhang, X., Gold, A.,
1237 Turpin, B. J., Thornton, J. A., Canagaratna, M. R. and Surratt, J. D.: Chemical Characterization
1238 of Secondary Organic Aerosol from Oxidation of Isoprene Hydroxyhydroperoxides, Environ.
1239 Sci. Technol., acs.est.6b02511–acs.est.6b02511, doi:10.1021/acs.est.6b02511, 2016.

1240 Riva, M., Chen, Y., Zhang, Y., Lei, Z., Olson, N. E., Boyer, H. C., Narayan, S., Yee, L. D.,
1241 Green, H. S., Cui, T., Zhang, Z., Baumann, K., Fort, M., Edgerton, E., Budisulistiorini, S. H.,
1242 Rose, C. A., Ribeiro, I. O., E Oliveira, R. L., Dos Santos, E. O., Machado, C. M. D., Szopa, S.,
1243 Zhao, Y., Alves, E. G., de Sá, S. S., Hu, W., Knipping, E. M., Shaw, S. L., Duvoisin Junior, S., de
1244 Souza, R. A. F., Palm, B. B., Jimenez, J.-L., Glasius, M., Goldstein, A. H., Pye, H. O. T., Gold,
1245 A., Turpin, B. J., Vizuete, W., Martin, S. T., Thornton, J. A., Dutcher, C. S., Ault, A. P. and
1246 Surratt, J. D.: Increasing Isoprene Epoxydiol-to-Inorganic Sulfate Aerosol Ratio Results in
1247 Extensive Conversion of Inorganic Sulfate to Organosulfur Forms: Implications for Aerosol
1248 Physicochemical Properties, Environ. Sci. Technol., 53(15), 8682–8694,
1249 doi:10.1021/acs.est.9b01019, 2019.

1250 Salcedo, D., Onasch, T. B., Aiken, a. C., Williams, L. R., de Foy, B., Cubison, M. J., Worsnop,
1251 D. R., Molina, L. T. and Jimenez, J. L.: Determination of particulate lead using aerosol mass
1252 spectrometry: MILAGRO/MCMA-2006 observations, Atmos. Chem. Phys., 10(12), 5371–5389,
1253 doi:10.5194/acp-10-5371-2010, 2010.

1254 Schindler, D. W.: Effects of Acid rain on freshwater ecosystems, Science, 239(4836), 149–157,
1255 doi:10.1126/science.239.4836.149, 1988.

1256 Schroder, J. C., Campuzano-Jost, P., Day, D. A., Shah, V., Larson, K., Sommers, J. M., Sullivan,
1257 A. P., Campos, T., Reeves, J. M., Hills, A., Hornbrook, R. S., Blake, N. J., Scheuer, E., Guo, H.,
1258 Fibiger, D. L., McDuffie, E. E., Hayes, P. L., Weber, R. J., Dibb, J. E., Apel, E. C., Jaeglé, L.,
1259 Brown, S. S., Thornton, J. A. and Jimenez, J. L.: Sources and Secondary Production of Organic
1260 Aerosols in the Northeastern United States during WINTER, J. Geophys. Res. D: Atmos., 42,
1261 4478, doi:10.1029/2018JD028475, 2018.

1262 Seinfeld, J. H. and Pandis, S. N.: Atmospheric Chemistry and Physics, 2nd ed., John Wiley &
1263 Sons, Inc., New York., 2006.

Song, S., Gao, M., Xu, W., Shao, J., Shi, G., Wang, S., Wang, Y., Sun, Y. and McElroy, M. B.: Fine-particle pH for Beijing winter haze as inferred from different thermodynamic equilibrium models, Atmos. Chem. Phys., 18(10), 7423–7438, doi:10.5194/acp-18-7423-2018, 2018.

Song, S., Gao, M., Xu, W., Sun, Y., Worsnop, D. R., Jayne, J. T., Zhang, Y., Zhu, L., Li, M., Zhou, Z. and Others: Possible heterogeneous chemistry of hydroxymethanesulfonate (HMS) in northern China winter haze, Atmos. Chem. Phys., 19(2), 1357–1371 [online] Available from: https://www.atmos-chem-phys.net/19/1357/2019/acp-19-1357-2019.pdf, 2019.

Sorooshian, A., Padró, L. T., Nenes, A., Feingold, G., McComiskey, A., Hersey, S. P., Gates, H., Jonsson, H. H., Miller, S. D., Stephens, G. L. and Others: On the link between ocean biota emissions, aerosol, and maritime clouds: Airborne, ground, and satellite measurements off the coast of California, Global Biogeochem. Cycles, 23(4) [online] Available from: https://agupubs.onlinelibrary.wiley.com/doi/abs/10.1029/2009GB003464, 2009.

Sorooshian, A., Crosbie, E., Maudlin, L. C., Youn, J.-S., Wang, Z., Shingler, T., Ortega, A. M., Hersey, S. and Woods, R. K.: Surface and airborne measurements of organosulfur and methanesulfonate over the western United States and coastal areas, J. Geophys. Res. D: Atmos., 120(16), 8535–8548, doi:10.1002/2015JD023822, 2015.

Stith, J. L., Ramanathan, V., Cooper, W. A., Roberts, G. C., DeMott, P. J., Carmichael, G., Hatch, C. D., Adhikary, B., Twohy, C. H., Rogers, D. C., Baumgardner, D., Prenni, A. J., Campos, T., Gao, R., Anderson, J. and Feng, Y.: An overview of aircraft observations from the Pacific Dust Experiment campaign, J. Geophys. Res., 114(D5), 833, doi:10.1029/2008JD010924, 2009.

Sueper, D.: ToF-AMS Data Analysis Software Webpage, [online] Available from: http://cires1.colorado.edu/jimenez-group/wiki/index.php/ ToF-AMS_Analysis_Software (Accessed 4 January 2017), 2018.

Surratt, J. D., Kroll, J. H., Kleindienst, T. E., Edney, E. O., Claeys, M., Sorooshian, A., Ng, N. L., Offenberg, J. H., Lewandowski, M., Jaoui, M., Flagan, R. C. and Seinfeld, J. H.: Evidence for organosulfates in secondary organic aerosol, Environ. Sci. Technol., 41(2), 517–527, doi:10.1021/es062081q, 2007.

Surratt, J. D., Gómez-González, Y., Chan, A. W. H., Vermeylen, R., Shahgholi, M., Kleindienst, T. E., Edney, E. O., Offenberg, J. H., Lewandowski, M., Jaoui, M., Maenhaut, W., Claeys, M., Flagan, R. C. and Seinfeld, J. H.: Organosulfate formation in biogenic secondary organic aerosol, J. Phys. Chem. A, 112(36), 8345–8378, doi:10.1021/jp802310p, 2008.

Thornton, J. A., Jaeglé, L. and McNeill, V. F.: Assessing known pathways for HO2 loss in aqueous atmospheric aerosols: Regional and global impacts on tropospheric oxidants, J. Geophys. Res. D: Atmos., 113(D5) [online] Available from: https://agupubs.onlinelibrary.wiley.com/doi/abs/10.1029/2007JD009236, 2008.

Tolocka, M. P. and Turpin, B.: Contribution of organosulfur compounds to organic aerosol mass, Environ. Sci. Technol., 46(15), 7978–7983, doi:10.1021/es300651v, 2012.

Toon, O. B., Maring, H., Dibb, J., Ferrare, R., Jacob, D. J., Jensen, E. J., Luo, Z. J., Mace, G. G., Pan, L. L., Pfister, L. and Others: Planning, implementation, and scientific goals of the Studies of Emissions and Atmospheric Composition, Clouds and Climate Coupling by Regional Surveys (SEAC4RS) field mission, J. Geophys. Res. D: Atmos., 121(9), 4967–5009 [online] Available from: https://agupubs.onlinelibrary.wiley.com/doi/abs/10.1002/2015JD024297%4010.1002/%28ISSN %292169-8996.SEAFOURC1, 2016.

Wagner, N. L., Brock, C. A., Angevine, W. M., Beyersdorf, A., Campuzano-Jost, P., Day, D., De Gouw, J. A., Diskin, G. S., Gordon, T. D., Graus, M. G. and Others: In situ vertical profiles of aerosol extinction, mass, and composition over the southeast United States during SENEX and SEAC 4 RS: observations of a modest aerosol enhancement aloft, Atmos. Chem. Phys., 15(12), 7085–7102 [online] Available from: https://www.atmos-chem-phys.net/15/7085/2015/acp-15-7085-2015.html, 2015.

Wang, Y., Zhang, Q., Jiang, J., Zhou, W., Wang, B., He, K., Duan, F., Zhang, Q., Philip, S. and Xie, Y.: Enhanced sulfate formation during China's severe winter haze episode in January 2013 missing from current models, J. Geophys. Res. D: Atmos., 119(17), 10–425 [online] Available from: https://agupubs.onlinelibrary.wiley.com/doi/abs/10.1002/2013JD021426, 2014.

Weber, R. J., Guo, H., Russell, A. G. and Nenes, A.: High aerosol acidity despite declining atmospheric sulfate concentrations over the past 15 years, Nat. Geosci., 9, 282, doi:10.1038/ngeo2665, 2016.

Wexler, A. S. and Clegg, S. L.: Atmospheric aerosol models for systems including the ions H+, NH4+, Na+, SO42-, NO3-, Cl-, Br-, and H2O, J. Geophys. Res. D: Atmos., 107(D14), ACH–14 [online] Available from: https://agupubs.onlinelibrary.wiley.com/doi/abs/10.1029/2001JD000451, 2002.

Youn, J.-S., Crosbie, E., Maudlin, L. C., Wang, Z. and Sorooshian, A.: Dimethylamine as a major alkyl amine species in particles and cloud water: Observations in semi-arid and coastal regions, Atmos. Environ. , 122, 250–258, doi:10.1016/j.atmosenv.2015.09.061, 2015.

Zhang, Q., Stanier, C. O., Canagaratna, M. R., Jayne, J. T., Worsnop, D. R., Pandis, S. N. and Jimenez, J. L.: Insights into the chemistry of new particle formation and growth events in Pittsburgh based on aerosol mass spectrometry, Environ. Sci. Technol., 38(18), 4797–4809, doi:10.1021/es035417u, 2004a.

Zhang, Q., Jimenez, J. L., Worsnop, D. R. and Canagaratna, M.: A case study of urban particle acidity and its influence on secondary organic aerosol, Environ. Sci. Technol., 41(9), 3213–3219, doi:10.1021/Es061812j, 2007a.

Zhang, Q., Jimenez, J. L., Canagaratna, M. R., Allan, J. D., Coe, H., Ulbrich, I., Alfarra, M. R., Takami, A., Middlebrook, A. M., Sun, Y. L. and Others: Ubiquity and dominance of oxygenated species in organic aerosols in anthropogenically-influenced Northern Hemisphere midlatitudes, Geophys. Res. Lett., 34(13) [online] Available from:

1339 https://agupubs.onlinelibrary.wiley.com/doi/abs/10.1029/2007GL029979%4010.1002/%28ISSN
1340 %291944-8007.GRL40, 2007b.

1341 Zhang, X., Smith, K. A., Worsnop, D. R., Jimenez, J. L., Jayne, J. T., Kolb, C. E., Morris, J. and
1342 Davidovits, P.: Numerical Characterization of Particle Beam Collimation: Part II Integrated
1343 Aerodynamic-Lens–Nozzle System, Aerosol Sci. Technol., 38(6), 619–638,
1344 doi:10.1080/02786820490479833, 2004b.

1345 Zheng, B., Zhang, Q., Zhang, Y., He, K. B., Wang, K., Zheng, G. J., Duan, F. K., Ma, Y. L. and
1346 Kimoto, T.: Heterogeneous chemistry: a mechanism missing in current models to explain
1347 secondary inorganic aerosol formation during the January 2013 haze episode in North China,
1348 Atmospheric Chemistry and Physics Discussions, 14(11), 16731–16776,
1349 doi:10.5194/acpd-14-16731-2014, 2014.

1350 Zheng, Y., Cheng, X., Liao, K., Li, Y., Li, Y., Huang, R.-J., Hu, W., Liu, Y., Zhu, T., Chen, S. and
1351 Others: Characterization of Anthropogenic Organic Aerosols by TOF-ACSM with the New
1352 Capture Vaporizer, Atmospheric Measurement Techniques [online] Available from:
1353 https://www.atmos-meas-tech-discuss.net/amt-2019-449/amt-2019-449.pdf, 2020.

1354 Zorn, S. R., Drewnick, F., Schott, M., Hoffmann, T. and Borrmann, S.: Characterization of the
1355 South Atlantic marine boundary layer aerosol using an aerodyne aerosol mass spectrometer,
1356 [online] Available from: https://hal.archives-ouvertes.fr/hal-00304023/, 2008.